



CERN-EP-2019-045
13 March 2019

Measurement of $p\bar{\Lambda} \oplus \bar{p}\Lambda$ and $\Lambda\bar{\Lambda}$ interactions with femtoscopic correlations in Pb–Pb collisions at $\sqrt{s_{NN}} = 2.76$ TeV and $\sqrt{s_{NN}} = 5.02$ TeV

ALICE Collaboration*

Abstract

Femtoscopic correlation functions were measured for $p\bar{p}$, $p\bar{\Lambda} \oplus \bar{p}\Lambda$, and $\Lambda\bar{\Lambda}$ pairs, as a function of collision centrality, in Pb–Pb collisions at $\sqrt{s_{NN}} = 2.76$ TeV and $\sqrt{s_{NN}} = 5.02$ TeV recorded by the ALICE experiment at the LHC. A simultaneous fit to all obtained correlation functions was performed, maximising the precision and sensitivity to the strong interaction parameters for the selected baryon pairs. Real and imaginary components of the scattering lengths, as well as the effective ranges, were extracted for combined $p\bar{\Lambda} \oplus \bar{p}\Lambda$ pairs and, for the first time, for $\Lambda\bar{\Lambda}$ pairs. Effective averaged scattering parameters for heavier baryon–anti-baryon pairs, not measured directly, are also provided. The results reveal similarly strong interaction between measured baryon–anti-baryon pairs, suggesting that they annihilate in the same manner as $p\bar{p}$ at the same pair relative momentum k^* . Moreover, the reported significant non-zero imaginary part and negative real part of the scattering length open up a possibility for future baryon–anti-baryon bound state searches.

arXiv:1903.06149v1 [nucl-ex] 14 Mar 2019

© 2019 CERN for the benefit of the ALICE Collaboration.

Reproduction of this article or parts of it is allowed as specified in the CC-BY-4.0 license.

*See Appendix A for the list of collaboration members

1 Introduction

The ALICE experiment [1] recorded collisions of Pb nuclei delivered by the the Large Hadron Collider (LHC) [2] at centre-of-mass energies of $\sqrt{s_{NN}} = 2.76$ TeV and $\sqrt{s_{NN}} = 5.02$ TeV.

Particle yields and their ratios measured in these collisions are well-described by Statistical Hadronisation Models (SHM's) [3–5], from which temperatures around 156 MeV and baryochemical potentials close to zero have been extracted [6]. The number of baryons created in each collision is of the order of one hundred and a similar number of anti-baryons is also created [7–9]. These include Λ , Σ , Ξ , and Ω and their corresponding anti-particles. The majority of them are produced at mid-rapidity and with low relative momentum: more than 95% of particles have p_T lower than 2 GeV/c. A Pb–Pb collision at the LHC can thus be viewed as a factory of low relative momentum baryon–anti-baryon pairs.

The interaction of baryons is a fundamental aspect of many sub-fields of nuclear physics. It is investigated extensively with numerous methods, including the detailed analysis of the properties of atomic nuclei as well as in dedicated experiments where beams of one baryon type are scattered on other baryons bound in atomic nuclei [10–15]. It is especially interesting to probe the interaction at low relative momenta. In particular, the possible creation of bound states for a given baryon–baryon pair was investigated extensively [16–21].

These techniques posses specific limitations depending on the properties of the interaction. Studies using nuclei are only possible for baryon combinations that create a bound system. It is therefore difficult to probe any kind of repulsive interaction in this way and it is also impossible to probe matter–anti-matter interaction with any of those methods. Scattering experiments can not be performed for any choice of baryon–baryon pairs and the available data are hampered by low statistics in the region of low relative momentum that is the most crucial for a precise extraction of the scattering parameters. As a result of these limitations, baryon interactions are well understood for nucleons and for the $p\bar{p}$ pair, but for baryons with non-zero strangeness and for baryon–anti-baryon pairs, data availability is limited.

The interactions of baryons are well known for pp pairs, for pn pairs, as well as for the lightest baryon–anti-baryon system, $p\bar{p}$ [22–26]. Measurements were also performed for $p\Lambda$ pairs [27–29]. The STAR Collaboration has recently performed a comparative study of the baryon–baryon and anti-baryon–anti-baryon interaction in Au–Au collisions at $\sqrt{s_{NN}} = 200$ GeV and found that the $p\bar{p}$ interaction does not differ from the pp system [30]. Also, ALICE measurements of the baryon–baryon pairs in pp collisions at $\sqrt{s} = 7$ TeV [31] shed more light on the interaction of $p\Lambda$ and $\Lambda\Lambda$ pairs at low relative pair momenta.

Concerning the baryon–anti-baryon pairs, the $p\bar{p}$ interaction is studied in detail in theory [23–26]. For other baryon–anti-baryon pairs however there are little or no experimental data available. For instance, the STAR experiment measured $p\bar{\Lambda} \oplus \bar{p}\Lambda$ correlations [32]; however, with several limitations: most importantly, no corrections for correlations arising from weak decays of heavier baryons were applied. Those baryon–anti-baryon scattering parameters, when measured, could be implemented in the the well-established model of heavy-ion collisions, UrQMD [33], which has the important feature of including rescattering in the hadronic phase. Especially, recent comparisons of theoretical calculations with the ALICE data show that a proper description of this phase is critical for the correct reproduction of a large number of observables, like particle yields, transverse-momentum spectra, femtосcopy for identified particles, as well as elliptic flow [34–37]. The baryon–anti-baryon annihilation is a critical component of the rescattering process. Yet, at the moment, for the heavier baryon–anti-baryon pairs, one has to rely on assumptions about the interaction cross section. Currently it is assumed that all baryon–anti-baryon pairs annihilate in the same way as $p\bar{p}$ pairs when taken at the same total energy of the pair, \sqrt{s} , in the pair rest frame [33]. In addition, the already mentioned STAR $p\bar{\Lambda} \oplus \bar{p}\Lambda$ correlation measurements [32], when reanalyzed taking into account residual correlations [38], suggest that all baryon–anti-baryon pairs might annihilate in a similar way as a function of the relative momentum of the pair k^* , instead of the pair centre-of-mass energy \sqrt{s} . This work aims to provide more experimental constraints on these scenarios.

The method of two-particle femtoscopy [39, 40], which is carried out in terms of the relative momenta of the particle pairs, allows one to access the baryon–anti-baryon interaction at low pair relative momentum in a way which is complementary to dedicated scattering experiments. This paper presents a femtoscopic analysis of $p\bar{p}$, $p\bar{\Lambda} \oplus \bar{p}\Lambda$, and $\Lambda\bar{\Lambda}$ correlations in Pb–Pb collisions at $\sqrt{s_{NN}} = 2.76$ TeV and $\sqrt{s_{NN}} = 5.02$ TeV measured by ALICE. The femtoscopic correlation functions represent the source function (probability to emit a particle from a given space–time point with a given momentum) seen through the specific interaction for a given pair. Only the strong interaction is present for $p\bar{\Lambda} \oplus \bar{p}\Lambda$ and $\Lambda\bar{\Lambda}$ pairs, while for $p\bar{p}$ pairs, where also the Coulomb interaction is present, it is the dominant contribution [41, 42]. Therefore, the parameters of this interaction, together with the source function, determine the shape of the correlation function. By fitting the measured correlation distributions with an appropriate function the strong interaction of baryon–anti-baryon pairs can be directly probed.

In the ALICE experiment, with its collider geometry, it is not always possible to experimentally distinguish on a particle-by-particle basis baryons which come directly from the collision region (“primary”) from the products of the weak decay of heavier hyperons (“secondary”). Therefore, in a measured baryon–anti-baryon pair sample, a certain number of pairs contain at least one non-primary particle. The femtoscopic correlation is formed on a timescale much smaller than the characteristic time of weak decays, so that such pairs will carry the information about the interaction of the parent particle. This correlation is then diluted by the decay kinematics and then combined with the femtoscopic correlation for all other pair types contributing to a given correlation function. This effect, called “residual correlations”, is accounted for in the formalism proposed in Ref. [38] which is employed in this analysis.

The measurement is performed for six centrality ranges and four pair types. At each centrality there is only one source function, which determines the system sizes for all pair types. The parameters of the strong interaction are independent of centrality. In addition, the measured pair types often share some of the possible parent particle combinations or are even parent pairs of other measured pairs (for example, the $\Lambda\bar{\Lambda}$ pair is measured, but on the one hand it is also a possible parent pair for a $p\bar{\Lambda}$ pair and therefore its correlation contributes to this system via the residual correlation mechanism). As a result, all measured correlation functions are non-trivially interconnected. Therefore, a procedure which is a single and simultaneous fit to all measured correlation functions is performed, with a single set of parameters for all of them. This provides maximum statistical accuracy for the obtained parameters, minimises the number of fit parameters and provides non-trivial internal consistency verification. Such a procedure is performed for the first time. The fit naturally includes the residual correlations mechanism. The formalism proposed in Ref. [38] does not treat this effect as a “contamination”. As a result, it does not attempt to “correct” for it (as proposed in an alternative procedure in Ref. [43]), but instead it uses it to extract information about the strong interaction potential parameters for the parent particles. Consequently, this measurement is also able to provide constraints on the effective strong interaction parameters for the pairs containing heavier baryons (such as $p\bar{\Xi}^+ \oplus \bar{p}\Xi^-$, etc.), not directly measured in this analysis.

The paper is organised as follows: in Sec. 2 the data-taking conditions, together with event and track selection criteria are described. The construction of the correlation function and the analysis procedure are described in Sec. 3. The fitting procedure is explained in Sec. 4. The estimation of the systematic uncertainty is discussed in Sec. 5. The femtoscopic correlation functions, as well as the extraction of the scattering parameters and associated systematic uncertainties are presented in Sec. 6. Section 7 concludes this paper.

2 Data analysis

2.1 Data sample

The data sample used in this work was collected in LHC Run 1 (2011) and Run 2 (2015), where two opposite beams of Pb nuclei were brought to collide at the centre-of-mass energy of $\sqrt{s_{NN}} = 2.76$ TeV and $\sqrt{s_{NN}} = 5.02$ TeV, respectively. Products of the collisions were measured by the ALICE detector. The performance of ALICE is described in Ref. [44].

In this analysis the minimum-bias (MB) trigger was used, which was based on the V0 detector consisting of two arrays of 32 scintillator counters, which are installed on each side of the interaction point and cover pseudorapidity ranges $2.8 < \eta < 5.1$ (V0A) and $-3.7 < \eta < -1.7$ (V0C). The MB trigger required a signal in both V0 detectors within a time window that is consistent with the collision occurring at the centre of the ALICE detector. Its efficiency for the centrality range used in this work is 100%. The event centrality was determined by analysing the signal from the V0 detector with the procedure described in details in Ref. [45].

The primary vertex location was reconstructed with the Inner Tracking System (ITS) [1]. The ITS is composed of six cylindrical layers of silicon detectors: two layers of Silicon Pixel Detectors (SPD) closest to the beam pipe with the acceptance of $|\eta| < 2.0$ and $|\eta| < 1.4$ for inner and outer layers, respectively, two layers of Silicon Drift Detectors (SDD) covering $|\eta| < 0.9$, and two outermost layers of Silicon Strip Detectors (SSD) covering $|\eta| < 1.0$. The information from the ITS can be used for tracking and primary vertex determination. However, in this analysis it was used only for the latter. The primary vertex for an event was required to be within ± 8 cm from the centre of the detector.

The analysis was performed in six centrality ranges for both collision energies. They are listed in Tab. 1 together with their corresponding average charged-particle multiplicity densities at mid-rapidity $\langle dN_{ch}/d\eta \rangle$ [45, 46].

Table 1: Centrality ranges and corresponding average charged-particle multiplicity densities at mid-rapidity $\langle dN_{ch}/d\eta \rangle$ for Pb–Pb collisions at $\sqrt{s_{NN}} = 2.76$ TeV [45] and $\sqrt{s_{NN}} = 5.02$ TeV [46].

Centrality	$\langle dN_{ch}/d\eta \rangle_{\sqrt{s_{NN}} = 2.76 \text{ TeV}}$	$\langle dN_{ch}/d\eta \rangle_{\sqrt{s_{NN}} = 5.02 \text{ TeV}}$
0–5%	1601 ± 60	1943 ± 53
5–10%	1294 ± 49	1586 ± 46
10–20%	966 ± 37	1180 ± 31
20–30%	649 ± 23	786 ± 20
30–40%	426 ± 15	512 ± 15
40–50%	261 ± 9	318 ± 12

2.2 Track selection

Particle trajectory (track) reconstruction for both collision energies was performed using the Time Projection Chamber (TPC) detector [47]. The TPC is divided by the central electrode into two halves. Each half is capped with a readout plane which is composed of 18 sectors (covering the full azimuthal angle ϕ) with 159 padrows placed radially in each sector. A track signal in the TPC consists of space points (clusters), and each of them is reconstructed in one of the padrows. A track was required to be composed of at least 80 clusters in order to select only good quality tracks and to minimise the possibility that a signal left by a single particle is reconstructed as two tracks. The parameters of the track are determined by performing a Kalman fit to a set of clusters. The quality of the fit is determined by calculating the χ^2 which was required to be lower than 4 for every cluster (each cluster has two d.o.f.), in order to select only well fitted tracks.

The identification of primary (anti-)protons was performed using the combined information from both the TPC and the Time-Of-Flight (TOF) detectors (a signal from both detectors was required), while the identification of Λ decay products (charged pions and protons) required information only from the TPC. The TOF is a cylindrical detector composed of 18 azimuthal sectors, further divided into five modules with Multigap Resistive Proportional Chambers (MRPC) along the beam axis, at a distance from the interaction point of $r \cong 380$ cm. Tracks are propagated from the TPC to the TOF and matched to hits in this detector. In the case of both TPC and TOF, the signals (energy loss dE/dx for the TPC and the time of flight for the TOF) were compared to the expected ones for a given particle. The measured–expected signal deviation was divided by the appropriate detector resolution σ . The track was accepted as a proton (pion) if it fell within 3σ of combined TPC and TOF expected signals for a proton (pion) in a given detector (see Tab. 2 for more details).

A pseudorapidity selection, $|\eta| < 0.8$, was applied to avoid regions of the detector with limited acceptance. The particle identification quality depends on the transverse momentum p_T , thus a choice of proper p_T range is needed to assure good purity of the sample (see Tab. 2 for details). To make sure that the sample is not significantly contaminated by secondary particles coming from weak decays and particle–detector interactions, a selection criterion on the Distance of Closest Approach (DCA) to the primary vertex was also applied, separately in the transverse plane (DCA_{xy}) and along the beam axis (DCA_z). These criteria were optimised in order to select a high purity sample of (anti-)protons. The p_T -integrated purity, based on Monte Carlo simulations, of the p (\bar{p}) sample was 95.4% (95.2%).

The selection of Λ ($\bar{\Lambda}$) was based on their distinctive decay topology (referred to as V^0) in the channel Λ ($\bar{\Lambda}$) $\rightarrow p\pi^-$ ($\bar{p}\pi^+$), with a branching ratio of 63.9% [22]. The reconstruction process, described in Ref. [48], is based on finding V^0 candidates made of two secondary tracks having opposite charge and large impact parameter with respect to the interaction point. If two V^0 candidates shared a daughter track, the V^0 candidate with the lowest DCA to the primary vertex was chosen, while the other one was rejected from the analysis. In addition, the particle identification using the combined information from the TPC and the TOF detectors, with the same selection criteria as the ones defined for primary tracks, was used. In order to calculate the purity of the Λ ($\bar{\Lambda}$) sample, the distribution of the invariant mass of the pairs was analysed. The signal S was approximated by a Gaussian superimposed on a second order polynomial background B [49]. Then, the Λ ($\bar{\Lambda}$) purity can be defined as $S/(S+B)$. In the invariant-mass range defined in Tab. 2 the p_T -integrated purity was found to be larger than 95%. All selection criteria for both primary and secondary tracks as well as V^0 candidates which were used in the analysis are summarised in Tab. 2.

In the $p\bar{p}$ analysis, the two-track selection criteria were chosen in order to reduce the effect of “split” tracks (a signal produced by one particle incorrectly reconstructed as two tracks) and “merged” tracks (a signal produced by two particles incorrectly reconstructed as one track). The effect can be quantified in the polar angle difference $\Delta\theta$, where it affects pairs with $\Delta\theta < 0.008$ rad, which were removed in the analysis. Moreover, tracks are bent by the magnetic field. Therefore, an azimuthal angle difference $\Delta\phi^*$ (where ϕ^* is a modified azimuthal angle ϕ , taking into account the bending of the track in the magnetic field [50]) was introduced and particle pairs which had $\Delta\phi^* < 0.012$ rad were removed from the analysis. In addition, pairs with pseudorapidity difference $\Delta\eta < 0.017$ were also removed from the final sample. A selection criterion based on “shared clusters” was also applied. Pairs, where the two tracks shared more than 5% of their clusters, were rejected. Moreover, the spatial separation for two tracks in each was measured at several points throughout the TPC (every 20 cm radially from 80 cm to 250 cm) and averaged. If the average separation of the like-sign tracks within a pair was below 5 cm, this pair was not taken into account in the analysis.

In the $p\bar{\Lambda} \oplus \bar{p}\Lambda$ analysis, a similar separation requirement between a same-sign primary proton and a secondary pion was set to 8 cm. For all other combinations of primary and secondary particles a 5 cm separation selection was used. In the $\Lambda\bar{\Lambda}$ analysis the minimum average separation between daughter

Table 2: Track and secondary vertex selection criteria.

Selection variable	Value
Common track selections	
$ \eta $	≤ 0.8
Number of TPC clusters	≥ 80
p (\bar{p}) transverse momentum p_T	$0.7 \leq p_T \leq 4.0 \text{ GeV}/c$
χ^2 per TPC cluster	≤ 4
Primary track selections	
DCA _{xy} to primary vertex	2.4 cm
DCA _z to primary vertex	3.2 cm
Particle identification	$\sqrt{N_{\sigma,\text{TPC}}^2 + N_{\sigma,\text{TOF}}^2} < 3$
Secondary track selections (Λ and $\bar{\Lambda}$ daughters)	
p (\bar{p}) daughter p_T	$0.5 \text{ (0.3)} \leq p_T \leq 4.0 \text{ (4.0)} \text{ GeV}/c$
π^- (π^+) daughter p_T	$0.16 \text{ (0.16)} \leq p_T \leq 4.0 \text{ (4.0)} \text{ GeV}/c$
Particle identification	$\sqrt{N_{\sigma,\text{TPC}}^2 + N_{\sigma,\text{TOF}}^2} < 3$
V^0 vertex selections (Λ and $\bar{\Lambda}$)	
$ \eta $	≤ 0.8
V^0 transverse momentum p_T	$0.7 \leq p_T \leq 5.0 \text{ GeV}/c$
DCA of V^0 to primary vertex	$\leq 0.5 \text{ cm}$
DCA between p (\bar{p}) and π^- (π^+) daughters	$\leq 0.4 \text{ cm}$
V^0 decay length	$\leq 60 \text{ cm}$
Cosine of V^0 pointing angle	≥ 0.9993
Λ ($\bar{\Lambda}$) mass acceptance window	$ m_{V^0} - m_{\Lambda\text{PDG}} \leq 0.0038 \text{ GeV}/c^2$
Minimum average separation in TPC	5.0 cm

tracks was set to 5 cm as well. The selections described above were able to minimise the “splitting” and “merging” effects in simulations.

3 Construction of the correlation function

The experimental correlation function $C(\vec{p}_1, \vec{p}_2)$ of two particles with three-momenta¹ \vec{p}_1 and \vec{p}_2 , respectively, is defined as

$$C(\vec{p}_1, \vec{p}_2) = \mathcal{N} \frac{A(\vec{p}_1, \vec{p}_2)}{B(\vec{p}_1, \vec{p}_2)}. \quad (1)$$

The distribution A , called the “signal”, is constructed from pairs of particles from the same event. The background distribution B is constructed from uncorrelated particles measured with the same single-particle acceptance. In this analysis it was built using the event mixing method with the two particles coming from two different events for which the vertex positions in the beam direction agree within 2 cm and the multiplicities differ by no more than 1/4 of the width of the given centrality class for which the correlation function is calculated. Each particle was correlated with particles from 10 other events. The parameter \mathcal{N} is the normalisation factor.

The femtoscopic correlation is measured as a function of the reduced momentum difference of the pair $\vec{k}^* = \frac{1}{2}(\vec{p}_1^* - \vec{p}_2^*)$, where \vec{p}_1^* and \vec{p}_2^* denote momenta of the two particles in the pair rest frame, as

¹Because all femtoscopic analyses are performed for identified particles, the particle masses are known; therefore, only three components of the four-momenta are independent.

$$C(\vec{k}^*) = \mathcal{N} \frac{A(\vec{k}^*)}{B(k^*)}. \quad (2)$$

In this work, the analysis is further simplified by performing all measurements as a function of the magnitude of the relative momentum $k^* = |\vec{k}^*|$ only. The \mathcal{N} parameter was calculated during the background subtraction procedure described in Sec. 4.3, in a way that the correlation function approaches unity in $k^* \in [0.13, 1.5]$ GeV/c for $p\bar{p}$ pairs and in $k^* \in [0.23, 1.5]$ GeV/c for $p\bar{\Lambda} \oplus \bar{p}\Lambda$ and $\Lambda\bar{\Lambda}$ pairs.

4 Fitting procedure

4.1 Fitting formula

The extraction of the scattering parameters from the measured correlation functions requires a dedicated fitting procedure, which takes into account the strong and Coulomb interaction, depending on a given pair. The fitting formula is chosen appropriately for each baryon–anti-baryon pair. Afterwards, a simultaneous fit to all measured pairs, taking into account residual correlations, is performed. The details of the procedure are described below.

In general, the theoretical two-particle correlation function is defined as [51, 52]

$$C(\vec{k}^*) = \int S(\vec{r}^*) \left| \Psi(\vec{k}^*, \vec{r}^*) \right|^2 d^3\vec{r}^*, \quad (3)$$

where $S(\vec{r}^*)$ is the source emission function, $\Psi(\vec{k}^*, \vec{r}^*)$ is the pair wave function, and \vec{r}^* is the relative separation vector. The source is assumed to have a spherically-symmetric Gaussian distribution. The pair wave function depends on the interactions between baryons and anti-baryons. When only the strong interaction is present, the Lednický–Lyuboshitz model is used [41]

$$C(k^*) = 1 + \sum_S \rho_S \left[\frac{1}{2} \left| \frac{f(k^*)}{r_0} \right|^2 \left(1 - \frac{d_0^S}{2\sqrt{\pi}r_0} \right) + \frac{2\Re f(k^*)}{\sqrt{\pi}r_0} F_1(2k^*r_0) - \frac{\Im f(k^*)}{r_0} F_2(2k^*r_0) \right], \quad (4)$$

where the sum is over all pair-spin configurations, with weights ρ_S (a real number) being 0.25 and 0.75 for singlet and triplet states, respectively, $f(k^*)$ (a complex function) is the scattering amplitude, r_0 (a real number) is the one-dimensional source size, d_0^S (a complex number) is the effective range for given spin configuration S , and $F_1(x)$ and $F_2(x)$ are known functions (for details see Ref. [41]). The scattering amplitude $f(k^*)$ in Eq. (4), in the effective range approximation, is defined as

$$f(k^*) = \left[\frac{1}{f_0^S} + \frac{1}{2} d_0^S k^{*2} - ik^* \right]^{-1}, \quad (5)$$

where f_0^S (a complex number) is the scattering length and d_0^S (a complex number) is the effective range of the interaction. In this work, the usual femtoscopic sign convention is employed when an attractive strong interaction is manifested as a positive real part of the scattering length $\Re f_0^S$. In addition, spin-averaged scattering parameters are extracted and the imaginary part of the effective range is set to be 0. Therefore, the final notation of extracted parameters is: $\Re f_0$ for the real part and $\Im f_0$ for the imaginary part of the spin-averaged scattering length, and d_0 for the real part of the spin-averaged effective range of the interaction. When the Coulomb interaction is also present, one has to numerically integrate the source emission function with the pair wave function containing a modified scattering amplitude [42].

Table 3: Fractions of residual components of $p\bar{p}$, $p\bar{\Lambda} \oplus \bar{p}\Lambda$, and $\Lambda\bar{\Lambda}$ correlation functions from AMPT (HIJING) after full detector simulation.

$p\bar{p}$		$p\bar{\Lambda} \oplus \bar{p}\Lambda$		$\Lambda\bar{\Lambda}$	
Pair	λ fraction	Pair	λ fraction	Pair	λ fraction
$p\bar{p}$	0.25 (0.32)	$p\bar{\Lambda}$	0.29 (0.28)	$\Lambda\bar{\Lambda}$	0.37 (0.24)
$p\bar{\Lambda}$	0.12 (0.19)	$\Lambda\bar{\Lambda}$	0.08 (0.09)	$\Lambda\bar{\Xi}^+$	0.04 (0.06)
$p\bar{\Sigma}^+$	0.04 (0.04)	$\Lambda\bar{\Sigma}^+$	0.03 (0.02)	$\Lambda\bar{\Xi}^0$	0.03 (0.05)
$\Lambda\bar{\Lambda}$	0.02 (0.03)	$p\bar{\Xi}^{0/+}$	0.02 (0.03)	$\Lambda\bar{\Sigma}^0$	< 0.01 (0.20)
$\Lambda\bar{\Sigma}^+$	0.01 (0.01)	$p\bar{\Sigma}^0$	< 0.01 (0.12)	$\Sigma^0\bar{\Sigma}^0$	< 0.01 (0.05)
$\Sigma^+\bar{\Sigma}^+$	< 0.01 (< 0.01)	$\Lambda\bar{\Sigma}^0$	< 0.01 (0.04)	$\Xi^{0/-}\bar{\Sigma}^0$	< 0.01 (0.02)
		$\Lambda\bar{\Xi}^{0/+}$	< 0.01 (0.01)	$\Xi^{0/-}\bar{\Xi}^{0/-}$	< 0.01 (< 0.01)
		$\Sigma^+\bar{\Sigma}^0$	< 0.01 (< 0.01)		
		$\Xi^{0/-}\bar{\Sigma}^+$	< 0.01 (< 0.01)		

4.2 Residual correlations

A fraction of observed (anti-)baryons comes from decays of heavier (anti-)baryons. In such a case, the correlation function is built for the daughter particles, while the interaction has taken place for the parent baryons. To account for this effect, a fitting formula contains a sum of correlation functions for each possible combination of (anti-)baryons, weighted by the fraction λ of given residual pairs. One needs to transform the theoretical correlation function of a pair into the momentum frame of the particles registered in the detector.

The procedure for the correlation function analysis taking into account residual correlations has been performed before and is described in detail in Ref. [53]. The same procedure was carried out in this analysis.

The fractions of residual pairs λ were calculated based on the AMPT model [54] after full detector simulation, estimating how many reconstructed pairs come from primary particles and what is the percentage of those coming from the given decay. They also take into account other impurities resulting from misidentification or detector effects. The obtained values of fractions are listed in Tab. 3. The momentum transformation matrices [38] were generated using the THERMINATOR 2 model [55] for all residual components of all analysed systems. The final correlation function for a xy pair is defined as

$$C_{xy}(k^*) = 1 + \sum_i \lambda_i [C_i(k^*) - 1], \quad (6)$$

where the sum is over all residual components of the xy pair and λ_i and $C_i(k^*)$ are the fraction and the correlation function of i -th pair, respectively [38].

4.3 Simultaneous fit to several pairs

The goal of this work is to extract the interaction parameters for various baryon–anti-baryon pairs. In order to increase the precision and robustness of this measurement, a procedure was developed to simultaneously fit correlation functions measured for different baryon–anti-baryon pairs.

A simultaneous fit is desirable because of the presence of residual correlations, which create a link between different pairs. For the $p\bar{p}$, $p\bar{\Lambda} \oplus \bar{p}\Lambda$ and $\Lambda\bar{\Lambda}$ systems studied in this paper, each measured corre-

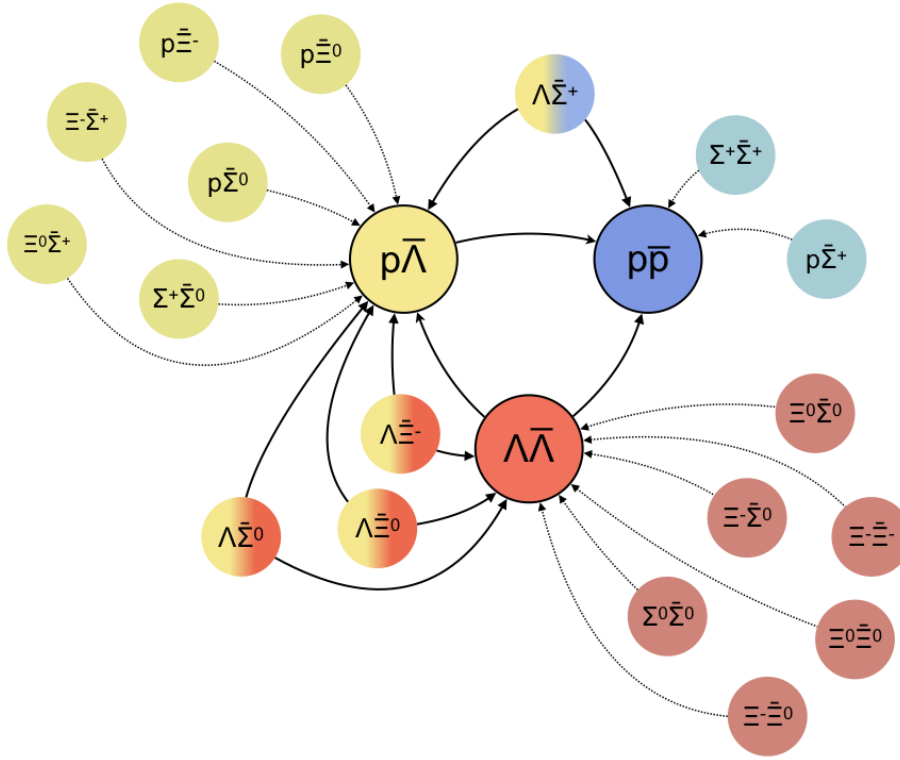


Figure 1: Illustration of the links between different baryon–anti-baryon pairs through the residual correlation mechanism.

lation is interlinked to the others via the complex net of residual correlations which is illustrated in Fig. 1. There are several pairs which are shared between different systems, for example major contributions affecting the $p\bar{p}$ correlation function are marked with blue, $p\bar{\Lambda}$ with yellow and $\Lambda\bar{\Lambda}$ with red. As can be seen in Fig. 1, there are several pairs which are shared between different systems. For instance, a fraction of pairs entering the $p\bar{p}$ correlation function come from the decays of Λ and $\bar{\Lambda}$ baryons. In this case, the interaction between Λ and $\bar{\Lambda}$ being manifested in the $p\bar{p}$ correlation function has the same parameters as the interaction of particles reconstructed and measured as a $\Lambda\bar{\Lambda}$ pair. In this example, those $\Lambda\bar{\Lambda}$ interaction parameters constitute a link between $p\bar{p}$ and $\Lambda\bar{\Lambda}$ correlation functions, allowing for a simultaneous fit of the two, with shared fit parameters. Moreover, this technique allows to provide constraints on those pairs which are not measured directly.

The femtoscopic correlation function is sensitive both to the interactions between particles and to the size of the emission source. As the focus of this study is the measurement of the baryon–anti-baryon interaction parameters, a number of assumptions concerning source sizes were made in order to increase the precision of the measurement.

The source radii for primary $p\bar{p}$, $p\bar{\Lambda} \oplus p\bar{\Lambda}$ and $\Lambda\bar{\Lambda}$ pairs were calculated from fits to previous measurements of other baryon–baryon and meson–meson pairs [53]. It was assumed that the one-dimensional source size R_{inv} , for each pair, depends on the transverse mass of the pair m_T , and event multiplicity N_{ch} . Event multiplicity is related to the volume of the overlapping region of the colliding nuclei (centrality), as particle production is proportional to the volume of the medium from which they are created [50].

The R_{inv} scaling with m_T follows the relation

$$R_{\text{inv}}(m_T; N_{\text{ch}}) = a(N_{\text{ch}}) \cdot m_T^\gamma, \quad (7)$$

where $a(N_{\text{ch}})$ and γ are empirical parameters obtained from the fit to the $R_{\text{inv}}(m_{\text{T}})$ dependence. The value of the exponent was found to be independent on centrality and fixed to $\gamma = 0.5$, while the exact values of $a(N_{\text{ch}})$ depend on the given centrality range. The same relation was used for the residual pairs, for which the transverse masses were calculated from transverse momentum spectra simulated in AMPT.

The R_{inv} scaling with event multiplicity N_{ch} was performed using the relation

$$R_{\text{inv}}(N_{\text{ch}}; m_{\text{T}}) = \alpha(m_{\text{T}}) \sqrt[3]{N_{\text{ch}}} + \beta(m_{\text{T}}), \quad (8)$$

where $\alpha(m_{\text{T}})$ and $\beta(m_{\text{T}})$ are empirical parameters and their exact values depend on the pair transverse mass (baryon–anti-baryon pair under consideration). The above relation can be further restricted when one notices that for a single particle the source size should be equal to the proton radius, which is $R_{\text{p}} \approx 0.88$ fm [22]. Finally, a set of scaling parameters and source radii was obtained for each pair under consideration (for each m_{T}) and for each centrality range.

The experimental correlation function is also affected by phenomena other than the strong and Coulomb interactions, such as jets and elliptic flow [56–58]. Those effects are treated as a background. For each experimental function, a background fit was performed in a k^* region where femtoscopic effects are not prominent. It was found, using THERMINATOR 2 model, that the results are not dependent on the k^* fit range when the background is fitted by a third order polynomial. Next, the estimated background was subtracted from the experimental correlation function. The procedure flattens the function for higher k^* and the slope is larger for less central collisions, which is consistent with elliptic flow, as it should be more prominent for semi-central collisions and less for central collisions [56].

Femtoscopic correlation functions were obtained for three baryon–anti-baryon pair systems $p\bar{p}$, $p\bar{\Lambda} \oplus \bar{p}\Lambda$, and $\Lambda\bar{\Lambda}$ in Pb–Pb collisions at two centre-of-mass collision energies $\sqrt{s_{\text{NN}}} = 2.76$ TeV and $\sqrt{s_{\text{NN}}} = 5.02$ TeV and in 6 centrality ranges. This yielded 36 measured correlation functions in total. The simultaneous fit, according to the procedure described above, was performed to all those pairs, with the $p\bar{p}$ scattering parameters fixed to the values previously measured [23]. Three sets of scattering parameters were introduced (each one containing a real and an imaginary part of the scattering length and an effective range) for $p\bar{\Lambda} \oplus \bar{p}\Lambda$, $\Lambda\bar{\Lambda}$ as well as heavier, not measured directly, baryon–anti-baryon pairs, which is denoted in further sections as BB . The correlation functions for $p\bar{p}$, $p\bar{\Lambda} \oplus \bar{p}\Lambda$, and $\Lambda\bar{\Lambda}$ pairs for the 10–20% centrality interval and two collision energies are represented together with the simultaneous fit in Fig. 2.

5 Systematic uncertainties

At the track selection level the analysis was also performed on tracks reconstructed using the information from both the ITS and the TPC, as opposed to those having the information from the TPC only. The correlation functions obtained from the analysis of those tracks were fitted with exactly the same procedure described in Sec. 4. Visible differences on extracted scattering parameters are between 4% and 17%, depending on the studied pair and the scattering parameter.

In addition, several components of the fit procedure were varied. Shifting the correlation function normalisation range in k^* by ± 0.1 GeV/ c yields almost no change on the extracted scattering parameters (maximum 1%). A change of the background parameterisation from the third to the fourth order polynomial results in differences of up to 19% for $\Im f_0$ and below 10% for other parameters. The second order polynomial was also tested but it fails to describe the low k^* region and therefore cannot be used to extract reliable information. Moreover, the use of residual pair fractions calculated from the HIJING model [59] instead of AMPT resulted in changes of up to 19% for d_0 , up to 16% for $\Im f_0$, and below 10% for $\Re f_0$. Variation of source sizes obtained from transverse mass and centrality scalings by $\pm 5\%$ resulted in changes of up to 13% for $\Re f_0$, up to 36% for $\Im f_0$, and up to 20% for d_0 .

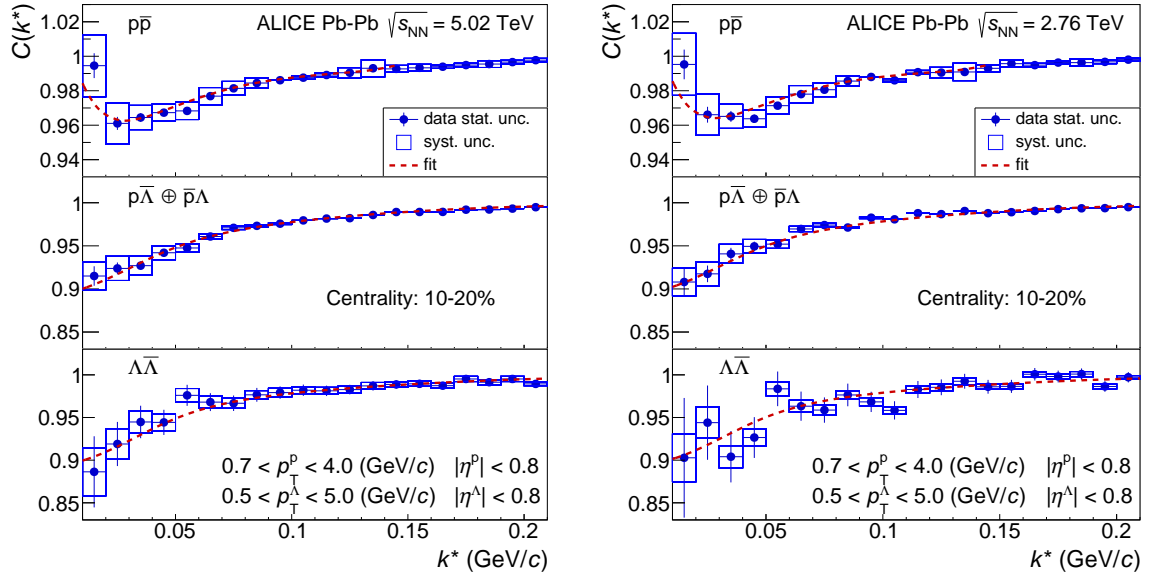


Figure 2: Correlation functions of $p\bar{p}$, $p\bar{\Lambda} \oplus \bar{p}\Lambda$, and $\Lambda\bar{\Lambda}$ pairs for Pb–Pb collisions at $\sqrt{s_{\text{NN}}} = 5.02$ TeV (left) and $\sqrt{s_{\text{NN}}} = 2.76$ TeV (right) together with the simultaneous femtoscopic fit for 10–20% centrality range.

The momentum resolution effect was investigated with Monte Carlo simulations by creating a two-dimensional matrix of generated and reconstructed k^* . Each slice of the distribution was then fitted with a Gaussian function. Within the k^* region of interest it was found that the width of the Gaussian function is constant; therefore, the fitting formula was smeared with a Gaussian with a width constant in k^* . The width of the Gaussian was varied by $\pm 30\%$ which results in systematic uncertainty of up to 11%.

Contributions to the systematic uncertainty on the extracted scattering parameters are summarised in Tab. 4. Since those components are correlated, the total systematic uncertainties are represented as covariance ellipses in the final plots.

6 Results

The results of the simultaneous fit to three baryon–anti-baryon pair combinations, $p\bar{p}$, $p\bar{\Lambda} \oplus \bar{p}\Lambda$, and $\Lambda\bar{\Lambda}$, are summarised in Tab. 5 and plotted in Fig. 3 together with statistical (bars) and systematic (ellipses) uncertainties. The comparison with values of the scattering parameters for various baryon–baryon and baryon–anti-baryon pairs extracted in previous experiments [60–63] are shown in Fig. 4.

As the simultaneous fit yields similar values, within uncertainties, of parameters for $p\bar{\Lambda} \oplus \bar{p}\Lambda$ and $\Lambda\bar{\Lambda}$, as well as heavier $B\bar{B}$ pairs, one can perform a fit assuming a single set of parameters for all systems. By doing so there is practically no change in the results; in particular, the $\chi^2 \approx 1.83$ ($p < 0.00001$) remains the same and other scattering parameters change very slightly, within systematic uncertainties. This test confirms that the data points can be correctly described when one assumes that all baryon–anti-baryon pairs have similar values of the scattering length and the effective range of the strong interaction.

The negative value of the real part of scattering length, $\Re f_0$, obtained for all baryon–anti-baryon pairs may have a twofold meaning – either the strong interaction is repulsive, or a bound state can be formed. The significant magnitude of the imaginary part of the scattering length, $\Im f_0$, shows that baryon–anti-baryon scattering may occur through inelastic processes (annihilation). In the UrQMD three scenarios can be considered [38]: i) all baryon–anti-baryon pairs annihilate similarly at the same pair transverse

Table 4: List of contributions to the systematic uncertainty of the scattering parameters. Values are averaged over collision energies and centrality ranges.

$p\bar{\Lambda} \oplus \bar{p}\Lambda$			
Uncertainty source	$\Re f_0$ (%)	$\Im f_0$ (%)	d_0 (%)
Normalisation range	< 1	< 1	< 1
Background parametrisation	< 1	2	3
Fit range dependence	3	8	14
Fractions of residual pairs	10	8	19
Momentum resolution correction	7	11	4
Track selection	11	14	4
Source size variation	9	18	20
$\Lambda\bar{\Lambda}$			
Uncertainty source	$\Re f_0$ (%)	$\Im f_0$ (%)	d_0 (%)
Normalisation range	< 1	< 1	< 1
Background parametrisation	6	19	2
Fit range dependence	2	4	5
Fractions of residual pairs	6	15	18
Momentum resolution correction	4	7	2
Track selection	7	17	4
Source size variation	12	35	19
$B\bar{B}$			
Uncertainty source	$\Re f_0$ (%)	$\Im f_0$ (%)	d_0 (%)
Normalisation range	< 1	1	1
Background parametrisation	6	17	6
Fit range dependence	6	12	11
Fractions of residual pairs	7	19	8
Momentum resolution correction	3	3	1
Track selection	9	< 1	12
Source size variation	13	36	9

momentum k^* ; ii) $\Im f_0$ is the same for all baryon–anti-baryon pairs, but expressed as a function of the pair centre-of-mass energy \sqrt{s} , meaning that $\Im f_0$ is smaller for baryon–anti-baryon pairs of higher total pair mass; iii) the inelastic cross section is increased for every matching quark–anti-quark pair in the baryon–anti-baryon system. In this scenario, in the specific case of this work, $\Im f_0$ for $p\bar{\Lambda} \oplus \bar{p}\Lambda$ should be lower than for $p\bar{p}$ and $\Lambda\bar{\Lambda}$, which is not observed. UrQMD by default uses scenario ii) to model the baryon–anti-baryon annihilation, which in our case would lead to a decrease of $\Im f_0$ while going from $p\bar{p}$ to $\Lambda\bar{\Lambda}$ pairs; however, similar values of $\Im f_0$ for all baryon–anti-baryon pairs reported in this work favour scenario i).

Inelastic scattering is compatible with a bound state, where the baryon and anti-baryon create a short-lived resonance which decays strongly into three particles. Evidence for a process in which a particle in the mass range of 2150–2260 MeV/ c^2 decays into a kaon and two pions has been reported by various experiments in the past and listed by the Particle Data Group (PDG) as $K_2(2250)$ [22]. The reported mass is slightly above the $p\bar{\Lambda}$ threshold, the width of the resonance is compatible with a strongly decaying system and the decay products match the valence quark content of the $p\bar{\Lambda}$ pair. A nucleon–anti-hyperon system has also been explicitly listed by PDG as $K_3(2320)$, with proton and $\bar{\Lambda}$ in the final state, which corresponds to the bound state undergoing an elastic scattering. Results presented in this paper support the existence of baryon–anti-baryon bound states such as $K_2(2250)$ and $K_3(2320)$. Further studies can

provide more evidence on the existence of those states.

Table 5: Values of the spin-averaged scattering parameters $\Re f_0$, $\Im f_0$, and d_0 for $p\bar{\Lambda} \oplus \bar{p}\Lambda$ and $\Lambda\bar{\Lambda}$ pairs, as well as effective parameters accounting for heavier baryon–anti-baryon ($B\bar{B}$) pairs not measured directly, extracted from the simultaneous fit. For comparison, $p\bar{p}$ scattering parameters from Ref. [23] fixed in the simultaneous fit are provided. Please note that the $p\bar{p}$ effective scattering parameters take into account the presence of the Coulomb interaction and coupled channels.

Parameter	$p\bar{p}$ (fixed from [23])	$p\bar{\Lambda} \oplus \bar{p}\Lambda$	$\Lambda\bar{\Lambda}$	$B\bar{B}$
$\Re f_0$ (fm)	-0.894 ± 0.051	$-1.15^{+0.23}_{-0.05}$ (syst.) (stat.)	$-0.90^{+0.16}_{-0.04}$ (syst.) (stat.)	$-1.08^{+0.11}_{-0.20}$ (syst.) (stat.)
$\Im f_0$ (fm)	0.88 ± 0.09	$0.53^{+0.15}_{-0.04}$ (syst.) (stat.)	$0.40^{+0.18}_{-0.06}$ (syst.) (stat.)	$0.57^{+0.25}_{-0.19}$ (syst.) (stat.)
d_0 (fm)	1.0	$3.06^{+0.98}_{-0.14}$ (syst.) (stat.)	$2.76^{+0.73}_{-0.29}$ (syst.) (stat.)	$2.69^{+0.46}_{-0.74}$ (syst.) (stat.)

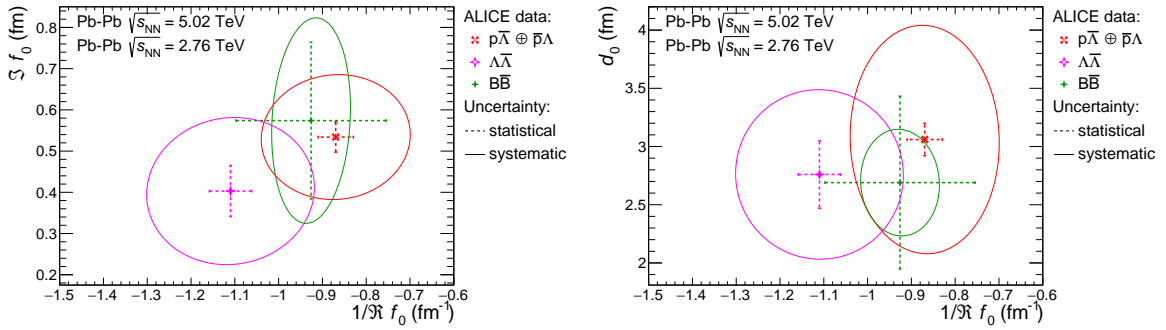


Figure 3: Extracted spin-averaged scattering parameters: (left) $\Re f_0$ and $\Im f_0$, (right) $\Re f_0$ and d_0 , for $p\bar{\Lambda} \oplus \bar{p}\Lambda$, $\Lambda\bar{\Lambda}$ pairs as well as effective scattering parameters for heavier baryon–anti-baryon ($B\bar{B}$) pairs not measured directly.

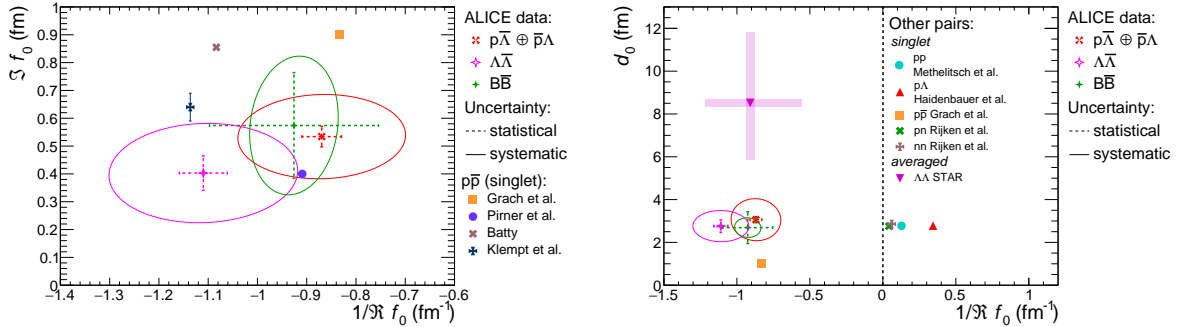


Figure 4: (Left) Comparison of extracted spin-averaged scattering parameters $\Re f_0$ and $\Im f_0$ for $p\bar{\Lambda} \oplus \bar{p}\Lambda$, $\Lambda\bar{\Lambda}$ pairs as well as effective $B\bar{B}$ pairs, with previous analyses of $p\bar{p}$ pairs (singlet) [23, 24, 26, 64]. (Right) Comparison of extracted spin-averaged scattering parameters $\Re f_0$ and d_0 for $p\bar{\Lambda} \oplus \bar{p}\Lambda$, $\Lambda\bar{\Lambda}$ pairs as well as effective $B\bar{B}$, with selected previous analyses of other pairs: pp (singlet) [65], $p\bar{p}$ (singlet) [64], pn (singlet) [66], nn (singlet) [66], $p\Lambda$ (singlet) [61], and $\Lambda\Lambda$ (spin-averaged) [62]. (Note that the $\Lambda\Lambda$ scattering parameters measured in the STAR experiment [62] did not account for residual correlations. The recent analysis of $\Lambda\Lambda$ correlations by the ALICE Collaboration [31], properly taking into account those correlations, disfavours the STAR parameters.)

7 Summary

Femtoscopic correlation functions for $p\bar{p}$, $p\bar{\Lambda} \oplus \bar{p}\Lambda$ and $\Lambda\bar{\Lambda}$ have been measured in Pb–Pb collisions at energies of $\sqrt{s_{NN}} = 2.76$ TeV and $\sqrt{s_{NN}} = 5.02$ TeV registered by the ALICE experiment. The analysis was performed in six centrality intervals, yielding a total number of 36 correlation functions.

A procedure was developed to allow for a simultaneous fit of all the obtained correlation functions. It includes a number of systematic checks to account for limited detector momentum resolution, non-femtoscopic background and residual correlations from feed-down of heavier baryons. In addition, assumptions were made concerning the scaling of the femtoscopic radii with multiplicity and with the transverse-momentum of a pair.

For the first time parameters of the strong interaction, the scattering length and the effective range, were extracted for $p\bar{\Lambda} \oplus \bar{p}\Lambda$ and $\Lambda\bar{\Lambda}$ pairs. Moreover, parameters for heavier baryon–anti-baryon pairs, which were not measured directly, are also provided.

Several conclusions can be drawn from the extracted parameters. First of all, it was found that the real and imaginary parts of the scattering length, $\Re f_0$ and $\Im f_0$, and the effective range of the interaction, d_0 , have similar values for all baryon–anti-baryon pairs. Therefore, the data points can be successfully described using the same parameters for all studied pairs.

A significant non-zero imaginary part of the scattering length, $\Im f_0$, is reported. It accounts for the presence of the inelastic channel of the interaction, which in the case of baryon–anti-baryon includes the annihilation process. The similarity of $\Im f_0$ between different pairs indicates that the dependence of the inelastic scattering cross section on the pair relative momentum k^* is the same, within systematic uncertainties, for all baryon–anti-baryon pairs. Note that the assumption used in UrQMD, that is a similar $\Im f_0$ for different baryon–anti-baryon pairs as a function of the centre-of-mass energy of the pair \sqrt{s} , means that the inelastic cross section would be different when taken at the same pair relative momentum k^* .

Finally, negative values of the extracted real part of the scattering length $\Re f_0$ show either that the interaction between baryon–anti-baryon pairs is repulsive, or that baryon–anti-baryon bound states can be formed. Combined with the non-zero imaginary part $\Im f_0$ which, as mentioned earlier, is associated with the inelastic processes, it favours the bound states scenario over the repulsive interaction. In that case a baryon–anti-baryon pair would form a resonance decaying into a group of particles different from the original ones (for instance, $p\bar{\Lambda} \rightarrow X \rightarrow K^+\pi^+\pi^-$, where X is the hypothetical baryon–anti-baryon bound state). Further studies will shed more light on existence of such particles.

Acknowledgements

The ALICE Collaboration would like to thank all its engineers and technicians for their invaluable contributions to the construction of the experiment and the CERN accelerator teams for the outstanding performance of the LHC complex. The ALICE Collaboration gratefully acknowledges the resources and support provided by all Grid centres and the Worldwide LHC Computing Grid (WLCG) collaboration. The ALICE Collaboration acknowledges the following funding agencies for their support in building and running the ALICE detector: A. I. Alikhanyan National Science Laboratory (Yerevan Physics Institute) Foundation (ANSL), State Committee of Science and World Federation of Scientists (WFS), Armenia; Austrian Academy of Sciences, Austrian Science Fund (FWF): [M 2467-N36] and Nationalstiftung für Forschung, Technologie und Entwicklung, Austria; Ministry of Communications and High Technologies, National Nuclear Research Center, Azerbaijan; Conselho Nacional de Desenvolvimento Científico e Tecnológico (CNPq), Universidade Federal do Rio Grande do Sul (UFRGS), Financiadora de Estudos e Projetos (Finep) and Fundação de Amparo à Pesquisa do Estado de São Paulo (FAPESP), Brazil; Ministry of Science & Technology of China (MSTC), National Natural Science Foundation of China (NSFC) and Ministry of Education of China (MOEC), China; Croatian Science Foundation and Ministry of Science and Education, Croatia; Centro de Aplicaciones Tecnológicas y Desarrollo Nuclear (CEADEN), Cubaenergía, Cuba; Ministry of Education, Youth and Sports of the Czech Republic, Czech Republic; The Danish Council for Independent Research — Natural Sciences, the Carlsberg Foundation and Danish National Research Foundation (DNRF), Denmark; Helsinki Institute of Physics (HIP), Finland;

Commissariat à l’Energie Atomique (CEA), Institut National de Physique Nucléaire et de Physique des Particules (IN2P3) and Centre National de la Recherche Scientifique (CNRS) and Région des Pays de la Loire, France; Bundesministerium für Bildung, Wissenschaft, Forschung und Technologie (BMBF) and GSI Helmholtzzentrum für Schwerionenforschung GmbH, Germany; General Secretariat for Research and Technology, Ministry of Education, Research and Religions, Greece; National Research, Development and Innovation Office, Hungary; Department of Atomic Energy Government of India (DAE), Department of Science and Technology, Government of India (DST), University Grants Commission, Government of India (UGC) and Council of Scientific and Industrial Research (CSIR), India; Indonesian Institute of Science, Indonesia; Centro Fermi - Museo Storico della Fisica e Centro Studi e Ricerche Enrico Fermi and Istituto Nazionale di Fisica Nucleare (INFN), Italy; Institute for Innovative Science and Technology, Nagasaki Institute of Applied Science (IIST), Japan Society for the Promotion of Science (JSPS) KAKENHI and Japanese Ministry of Education, Culture, Sports, Science and Technology (MEXT), Japan; Consejo Nacional de Ciencia (CONACYT) y Tecnología, through Fondo de Cooperación Internacional en Ciencia y Tecnología (FONCICYT) and Dirección General de Asuntos del Personal Académico (DGAPA), Mexico; Nederlandse Organisatie voor Wetenschappelijk Onderzoek (NWO), Netherlands; The Research Council of Norway, Norway; Commission on Science and Technology for Sustainable Development in the South (COMSATS), Pakistan; Pontificia Universidad Católica del Perú, Peru; Ministry of Science and Higher Education and National Science Centre, Poland; Korea Institute of Science and Technology Information and National Research Foundation of Korea (NRF), Republic of Korea; Ministry of Education and Scientific Research, Institute of Atomic Physics and Ministry of Research and Innovation and Institute of Atomic Physics, Romania; Joint Institute for Nuclear Research (JINR), Ministry of Education and Science of the Russian Federation, National Research Centre Kurchatov Institute, Russian Science Foundation and Russian Foundation for Basic Research, Russia; Ministry of Education, Science, Research and Sport of the Slovak Republic, Slovakia; National Research Foundation of South Africa, South Africa; Swedish Research Council (VR) and Knut & Alice Wallenberg Foundation (KAW), Sweden; European Organization for Nuclear Research, Switzerland; National Science and Technology Development Agency (NSDTA), Suranaree University of Technology (SUT) and Office of the Higher Education Commission under NRU project of Thailand, Thailand; Turkish Atomic Energy Agency (TAEK), Turkey; National Academy of Sciences of Ukraine, Ukraine; Science and Technology Facilities Council (STFC), United Kingdom; National Science Foundation of the United States of America (NSF) and United States Department of Energy, Office of Nuclear Physics (DOE NP), United States of America.

References

- [1] ALICE Collaboration, K. Aamodt *et al.*, “The ALICE experiment at the CERN LHC”, *JINST* **3** (2008).
- [2] L. Evans and P. Bryant, “LHC Machine”, *JINST* **3** (2008).
- [3] A. Andronic, P. Braun-Munzinger, and J. Stachel, “Hadron production in central nucleus-nucleus collisions at chemical freeze-out”, *Nucl. Phys.* **A772** (2006), arXiv:nucl-th/0511071 [nucl-th].
- [4] F. Becattini and R. Fries, “The QCD confinement transition: Hadron formation”, *Landolt-Bornstein* **23** (2010), arXiv:0907.1031 [nucl-th].
- [5] J. Cleymans and K. Redlich, “Unified description of freezeout parameters in relativistic heavy ion collisions”, *Phys. Rev. Lett.* **81** (1998), arXiv:nucl-th/9808030 [nucl-th].
- [6] A. Andronic, P. Braun-Munzinger, K. Redlich, and J. Stachel, “The thermal model on the verge of

- the ultimate test: particle production in Pb–Pb collisions at the LHC”, *J. Phys.* **G38** (2011), arXiv:1106.6321 [nucl-th].
- [7] ALICE Collaboration, B. Abelev *et al.*, “ K_S^0 and Λ production in Pb–Pb collisions at $\sqrt{s_{NN}} = 2.76$ TeV”, *Phys. Rev. Lett.* **111** (2013), arXiv:1307.5530 [nucl-ex].
- [8] ALICE Collaboration, B. Abelev *et al.*, “Pion, kaon, and proton production in central Pb–Pb collisions at $\sqrt{s_{NN}} = 2.76$ TeV”, *Phys. Rev. Lett.* **109** (2012), arXiv:1208.1974 [hep-ex].
- [9] ALICE Collaboration, B. Abelev *et al.*, “Centrality dependence of π , K, p production in Pb–Pb collisions at $\sqrt{s_{NN}} = 2.76$ TeV”, *Phys. Rev.* **C88** (2013), arXiv:1303.0737 [hep-ex].
- [10] V. G. J. Stoks, R. A. M. Klomp, M. C. M. Rentmeester, and J. J. de Swart, “Partial wave analysis of all nucleon–nucleon scattering data below 350 MeV”, *Phys. Rev.* **C48** (1993).
- [11] r. Engelmann, H. Filthuth, V. Hepp, and E. Kluge, “Inelastic Σ^-p -interactions at low momenta”, *Phys. Rev.* **21** (1966).
- [12] F. Eisele, H. Filthuth, W. Foehlich, V. Hepp, and G. Zech, “Elastic $\Sigma^\pm p$ scattering at low energies”, *Phys. Lett.* **37B** (1971).
- [13] V. Hepp and H. Schleich, “A new determination of the capture ratio $r(c) = \Sigma^-p \rightarrow \Sigma^0n / (\Sigma^-p \rightarrow \Sigma^0n) + (\Sigma^-p \rightarrow \Lambda n)$, the Λ^0 lifetime and $\Sigma^- \Lambda^0$ mass difference”, *Z. Phys.* **214** (1968).
- [14] J. de Swart and C. Dullemond, “Effective range theory and the low energy hyperon–nucleon interactions”, *Annals of Physics* **19** (1962).
- [15] S. Bart *et al.*, “Sigma hyperons in the nucleus”, *Phys. Rev. Lett.* **83** (1999).
- [16] O. Hashimoto and H. Tamura, “Spectroscopy of lambda hypernuclei”, *Prog. Part. Nucl. Phys.* **57** (2006).
- [17] R. S. Hayano, T. Ishikawa, M. Iwasaki, H. Outa, E. Takada, H. Tamura, A. Sakaguchi, M. Aoki, and T. Yamazaki, “Observation of a bound state of ^4He (Σ) hypernucleus”, *Phys. Lett.* **B231** (1989).
- [18] T. Nagae, T. Miyachi, T. Fukuda, H. Outa, T. Tamagawa, J. Nakano, R. S. Hayano, H. Tamura, Y. Shimizu, K. Kubota, R. E. Chrien, R. Sutter, A. Rusek, W. J. Briscoe, R. Sawafuta, E. V. Hungerford, A. Empl, W. Naing, C. Neerman, K. Johnston, and M. Planinic, “Observation of a ^4He bound state in the $^4\text{He}(K^-, \pi^-)$ reaction at 600 MeV/c”, *Phys. Rev. Lett.* **80** (1998).
- [19] K. Nakazawa, Y. Endo, S. Fukunaga, K. Hoshino, S. H. Hwang, K. Imai, H. Ito, K. Itonaga, T. Kanda, M. Kawasaki, J. H. Kim, S. Kinbara, H. Kobayashi, A. Mishina, S. Ogawa, H. Shibuya, T. Sugimura, M. K. Soe, H. Takahashi, T. Takahashi, K. T. Tint, K. Umehara, C. S. Yoon, and J. Yoshida, “The first evidence of a deeply bound state of $\xi^- - ^{14}\text{n}$ system”, *Progress of Theoretical and Experimental Physics* **2015**.
- [20] R. L. Jaffe, “Perhaps a stable dihyperon”, *Phys. Rev. Lett.* **38** (1977). [Erratum: *Phys. Rev. Lett.* **38** (1977), 617].
- [21] H. Takahashi *et al.*, “Observation of a $(\Lambda\Lambda)\text{He-6}$ double hypernucleus”, *Phys. Rev. Lett.* **87** (2001).
- [22] Particle Data Group Collaboration, C. Patrignani *et al.*, “Review of Particle Physics”, *Chin. Phys.* **C40** (2016).

- [23] C. J. Batty, “Anti-protonic hydrogen atoms”, *Rept. Prog. Phys.* **52** (1989).
- [24] H. Pirner, B. Kerbikov, and J. Mahalanabis, “Updating the effective range expansion of low-energy N– anti-N scattering”, *Z.Phys.* **A338** (1991).
- [25] I. L. Grach, B. O. Kerbikov, and Yu. A. Simonov, “Nucleon–anti-nucleon low-energy interaction in the effective range approximation”, *Sov. J. Nucl. Phys.* **48** (1988) . [*Yad. Fiz.*48,956(1988)].
- [26] E. Klempt, F. Bradamante, A. Martin, and J. Richard, “Anti-nucleon–nucleon interaction at low energy: scattering and protonium”, *Phys. Rept.* **368** (2002).
- [27] G. Alexander, U. Karshon, A. Shapira, G. Yekutieli, R. Engelmann, H. Filthuth, and W. Lughofer, “Study of the Λ –N system in low-energy Λ –p elastic scattering”, *Phys. Rev.* **173** (1968).
- [28] B. Sechi-Zorn, B. Kehoe, J. Twitty, and R. A. Burnstein, “Low-energy lambda–proton elastic scattering”, *Phys. Rev.* **175** (1968).
- [29] J. A. Kadyk, G. Alexander, J. H. Chan, P. Gaposchkin, and G. H. Trilling, “ Λ p interactions in momentum range 300 to 1500 MeV/c”, *Nucl. Phys.* **B27** (1971).
- [30] **STAR** Collaboration, L. Adamczyk *et al.*, “Measurement of interaction between antiprotons”, *Nature* **527** (2015), arXiv:1507.07158 [nucl-ex].
- [31] **ALICE** Collaboration, S. Acharya *et al.*, “p–p, p– Λ and Λ – Λ correlations studied via femtoscopy in pp reactions at $\sqrt{s} = 7$ TeV”, *Phys. Rev.* **C99** (2019), arXiv:1805.12455 [nucl-ex].
- [32] **STAR** Collaboration, J. Adams *et al.*, “Proton– Λ correlations in central Au+Au collisions at $\sqrt{s_{NN}} = 200$ GeV”, *Phys. Rev.* **C74** (2006), arXiv:nucl-ex/0511003 [nucl-ex].
- [33] M. Bleicher *et al.*, “Relativistic hadron–hadron collisions in the ultrarelativistic quantum molecular dynamics model”, *J. Phys.* **G25** (1999), arXiv:hep-ph/9909407 [hep-ph].
- [34] J. Steinheimer, J. Aichelin, and M. Bleicher, “Nonthermal p/ π Ratio at LHC as a consequence of hadronic final state interactions”, *Phys. Rev. Lett.* **110** (2013), arXiv:1203.5302 [nucl-th].
- [35] J. Steinheimer, J. Aichelin, M. Bleicher, and H. Stcker, “Influence of the hadronic phase on observables in ultrarelativistic heavy ion collisions”, *Phys. Rev.* **C95** (2017), arXiv:1703.06638 [nucl-th].
- [36] K. Werner, I. Karpenko, M. Bleicher, T. Pierog, and S. Porteboeuf-Houssais, “Jets, bulk matter, and their interaction in heavy-ion collisions at several TeV”, *Phys. Rev.* **C85** (2012), arXiv:1203.5704 [nucl-th].
- [37] I. A. Karpenko, Yu. M. Sinyukov, and K. Werner, “Uniform description of bulk observables in the hydrokinetic model of $A + A$ collisions at the BNL Relativistic Heavy Ion Collider and the CERN Large Hadron Collider”, *Phys. Rev.* **C87** (2013), arXiv:1204.5351 [nucl-th].
- [38] A. Kisiel, H. Zbroszczyk, and M. Szymaski, “Extracting baryon-antibaryon strong interaction potentials from $p\bar{\Lambda}$ femtoscopic correlation functions”, *Phys. Rev.* **C89** (2014), arXiv:1403.0433 [nucl-th].
- [39] R. Lednicky, “Correlation femtoscopy”, *Nucl. Phys.* **A774** (2006), arXiv:nucl-th/0510020 [nucl-th].
- [40] M. A. Lisa, S. Pratt, R. Soltz, and U. Wiedemann, “Femtoscopy in relativistic heavy ion collisions”, *Ann. Rev. Nucl. Part. Sci.* **55** (2005), arXiv:nucl-ex/0505014 [nucl-ex].

- [41] R. Lednicky and V. Lyuboshits, “Final state interaction effect on pairing correlations between particles with small relative momenta”, *Sov.J.Nucl.Phys.* **35** (1982) .
- [42] R. Lednicky, “Finite-size effects on two-particle production in continuous and discrete spectrum”, *Phys. Part. Nucl.* **40** (2009) , arXiv:nucl-th/0501065 [nucl-th].
- [43] V. M. Shapoval, B. Erazmus, R. Lednicky, and Yu. M. Sinyukov, “Extracting $p\Lambda$ scattering lengths from heavy ion collisions”, *Phys. Rev.* **C92** (2015) , arXiv:1405.3594 [nucl-th].
- [44] ALICE Collaboration, B. Abelev *et al.*, “Performance of the ALICE Experiment at the CERN LHC”, *Int. J. Mod. Phys.* **A29** (2014) , arXiv:1402.4476 [nucl-ex].
- [45] ALICE Collaboration, K. Aamodt *et al.*, “Centrality dependence of the charged-particle multiplicity density at mid-rapidity in Pb-Pb collisions at $\sqrt{s_{NN}} = 2.76$ TeV”, *Phys. Rev. Lett.* **106** (2011) , arXiv:1012.1657 [nucl-ex].
- [46] ALICE Collaboration, J. Adam *et al.*, “Centrality dependence of the charged-particle multiplicity density at midrapidity in Pb-Pb collisions at $\sqrt{s_{NN}} = 5.02$ TeV”, *Phys. Rev. Lett.* **116** no. 22, (2016) , arXiv:1512.06104 [nucl-ex].
- [47] J. Alme *et al.*, “The ALICE TPC, a large 3-dimensional tracking device with fast readout for ultra-high multiplicity events”, *Nucl. Instrum. Meth.* **A622** (2010) , arXiv:1001.1950 [physics.ins-det].
- [48] ALICE Collaboration, C. W. Fabjan *et al.*, “ALICE: Physics Performance Report, Volume II”, *J. Phys.* **G32** (2006) .
- [49] ALICE Collaboration, K. Aamodt *et al.*, “Strange particle production in proton-proton collisions at $\sqrt{s} = 0.9$ TeV with ALICE at the LHC”, *Eur. Phys. J.* **C71** (2011) , arXiv:1012.3257 [hep-ex].
- [50] ALICE Collaboration, J. Adam *et al.*, “Centrality dependence of pion freeze-out radii in Pb–Pb collisions at $\sqrt{s_{NN}} = 2.76$ TeV”, *Phys. Rev.* **C93** (2016) , arXiv:1507.06842 [nucl-ex].
- [51] S. E. Koonin, “Proton pictures of high-energy nuclear collisions”, *Phys. Lett.* **B70** (1977) .
- [52] S. Pratt, T. Csorgo, and J. Zimanyi, “Detailed predictions for two pion correlations in ultrarelativistic heavy-ion collisions”, *Phys. Rev.* **C42** (1990) .
- [53] ALICE Collaboration, J. Adam *et al.*, “One-dimensional pion, kaon, and proton femtосopy in Pb–Pb collisions at $\sqrt{s_{NN}} = 2.76$ TeV”, *Phys. Rev.* **C92** no. 5, (2015) , arXiv:1506.07884 [nucl-ex].
- [54] Z.-W. Lin, C. M. Ko, B.-A. Li, B. Zhang, and S. Pal, “A Multi-phase transport model for relativistic heavy ion collisions”, *Phys. Rev.* **C72** (2005) , arXiv:nucl-th/0411110 [nucl-th].
- [55] M. Chojnacki, A. Kisiel, W. Florkowski, and W. Broniowski, “THERMINATOR 2: THERMal heavy IoN generATOR 2”, *Comput. Phys. Commun.* **183** (2012) , arXiv:1102.0273 [nucl-th].
- [56] A. Kisiel, “Non-identical particle correlation analysis in the presence of non-femtoscopic correlations”, *Acta Phys. Polon.* **B48** (2017) .
- [57] ALICE Collaboration, K. Aamodt *et al.*, “Femtосopy of pp collisions at $\sqrt{s} = 0.9$ and 7 TeV at the LHC with two-pion Bose-Einstein correlations”, *Phys. Rev.* **D84** (2011) , arXiv:1101.3665 [hep-ex].

- [58] L. K. Graczykowski, A. Kisiel, M. A. Janik, and P. Karczmarczyk, “Extracting femtoscopic radii in the presence of significant additional correlation sources”, *Acta Phys. Polon.* **B45** (2014), arXiv:1409.8120 [nucl-th].
- [59] X.-N. Wang and M. Gyulassy, “HIJING: A Monte Carlo model for multiple jet production in pp, pA and AA collisions”, *Phys. Rev.* **D44** (1991).
- [60] B. Kerbikov, A. Stavinsky, and V. Fedotov, “Model independent view on the low mass proton anti-proton enhancement”, *Phys. Rev.* **C69** (2004), arXiv:hep-ph/0402054 [hep-ph].
- [61] J. Haidenbauer, S. Patschauer, N. Kaiser, U. G. Meissner, A. Nogga, and W. Weise, “Hyperon-nucleon interaction at next-to-leading order in chiral effective field theory”, *Nucl. Phys.* **A915** (2013), arXiv:1304.5339 [nucl-th].
- [62] STAR Collaboration, L. Adamczyk *et al.*, “ $\Lambda\bar{\Lambda}$ Correlation Function in Au+Au collisions at $\sqrt{s_{NN}} = 200$ GeV”, *Phys. Rev. Lett.* **114** no. 2, (2015), arXiv:1408.4360 [nucl-ex].
- [63] E. Czerwinski *et al.*, “Determination of the η' -p scattering length in free space”, *Phys. Rev. Lett.* **113** (2014), arXiv:1404.5436 [nucl-ex].
- [64] I. L. Grach, B. O. Kerbikov, and Yu. A. Simonov, “Effective Range Analysis of Low-energy Nucleon - Anti-nucleon Interaction”, *Phys. Lett.* **B208** (1988).
- [65] L. Mathelitsch and B. J. Verwest, “Effective range parameters in nucleon–nucleon scattering”, *Phys. Rev.* **C29** (1984).
- [66] T. A. Rijken, M. Nagels, and Y. Yamamoto, “Baryon–baryon interactions: Nijmegen extended-soft-core models”, *Prog.Theor.Phys.Suppl.* **185** (2010).

A The ALICE Collaboration

S. Acharya¹⁴¹, D. Adamová⁹³, S.P. Adhya¹⁴¹, A. Adler⁷⁴, J. Adolfsson⁸⁰, M.M. Aggarwal⁹⁸, G. Aglieri Rinella³⁴, M. Agnello³¹, N. Agrawal¹⁰, Z. Ahammed¹⁴¹, S. Ahmad¹⁷, S.U. Ahn⁷⁶, S. Aiola¹⁴⁶, A. Akindinov⁶⁴, M. Al-Turany¹⁰⁵, S.N. Alam¹⁴¹, D.S.D. Albuquerque¹²², D. Aleksandrov⁸⁷, B. Alessandro⁵⁸, H.M. Alfandá⁶, R. Alfaro Molina⁷², B. Ali¹⁷, Y. Ali¹⁵, A. Alici^{10,53,27}, A. Alkin², J. Alme²², T. Alt⁶⁹, L. Altenkamper²², I. Altsybeev¹¹², M.N. Anaam⁶, C. Andrei⁴⁷, D. Andreou³⁴, H.A. Andrews¹⁰⁹, A. Andronic^{105,144}, M. Angeletti³⁴, V. Anguelov¹⁰², C. Anson¹⁶, T. Antičić¹⁰⁶, F. Antinori⁵⁶, P. Antonioli⁵³, R. Anwar¹²⁶, N. Apadula⁷⁹, L. Aphecetche¹¹⁴, H. Appelshäuser⁶⁹, S. Arcelli²⁷, R. Arnaldi⁵⁸, M. Arratia⁷⁹, I.C. Arsene²¹, M. Arslandok¹⁰², A. Augustinus³⁴, R. Averbeck¹⁰⁵, S. Aziz⁶¹, M.D. Azmi¹⁷, A. Badalà⁵⁵, Y.W. Baek^{60,40}, S. Bagnasco⁵⁸, R. Bailhache⁶⁹, R. Bala⁹⁹, A. Baldisseri¹³⁷, M. Ball⁴², R.C. Baral⁸⁵, R. Barbera²⁸, L. Barioglio²⁶, G.G. Barnaföldi¹⁴⁵, L.S. Barnby⁹², V. Barret¹³⁴, P. Bartalini⁶, K. Barth³⁴, E. Bartsch⁶⁹, N. Bastid¹³⁴, S. Basu¹⁴³, G. Batigne¹¹⁴, B. Batyunya⁷⁵, P.C. Batzing²¹, D. Bauri⁴⁸, J.L. Bazo Alba¹¹⁰, I.G. Bearden⁸⁸, C. Bedda⁶³, N.K. Behera⁶⁰, I. Belikov¹³⁶, F. Bellini³⁴, R. Bellwied¹²⁶, L.G.E. Beltran¹²⁰, V. Belyaev⁹¹, G. Bencedi¹⁴⁵, S. Beole²⁶, A. Bercuci⁴⁷, Y. Berdnikov⁹⁶, D. Berenyi¹⁴⁵, R.A. Bertens¹³⁰, D. Berzano⁵⁸, L. Betev³⁴, A. Bhasin⁹⁹, I.R. Bhat⁹⁹, H. Bhatt⁴⁸, B. Bhattacharjee⁴¹, A. Bianchi²⁶, L. Bianchi^{126,26}, N. Bianchi⁵¹, J. Bielčák³⁷, J. Bielčková⁹³, A. Bilandzic^{103,117}, G. Biro¹⁴⁵, R. Biswas³, S. Biswas³, J.T. Blair¹¹⁹, D. Blau⁸⁷, C. Blume⁶⁹, G. Boca¹³⁹, F. Bock³⁴, A. Bogdanov⁹¹, L. Boldizsár¹⁴⁵, A. Bolozdynya⁹¹, M. Bombara³⁸, G. Bonomi¹⁴⁰, M. Bonora³⁴, H. Borel¹³⁷, A. Borissov^{144,91}, M. Borri¹²⁸, E. Botta²⁶, C. Bourjau⁸⁸, L. Bratrud⁶⁹, P. Braun-Munzinger¹⁰⁵, M. Bregant¹²¹, T.A. Broker⁶⁹, M. Broz³⁷, E.J. Brucken⁴³, E. Bruna⁵⁸, G.E. Bruno^{33,104}, M.D. Buckland¹²⁸, D. Budnikov¹⁰⁷, H. Buesching⁶⁹, S. Bufalino³¹, O. Bugnon¹¹⁴, P. Buhler¹¹³, P. Buncic³⁴, O. Busch^{133,i}, Z. Buthelezi⁷³, J.B. Butt¹⁵, J.T. Buxton⁹⁵, D. Caffarri⁸⁹, A. Caliva¹⁰⁵, E. Calvo Villar¹¹⁰, R.S. Camacho⁴⁴, P. Camerini²⁵, A.A. Capon¹¹³, F. Carnesecchi¹⁰, J. Castillo Castellanos¹³⁷, A.J. Castro¹³⁰, E.A.R. Casula⁵⁴, F. Catalano³¹, C. Ceballos Sanchez⁵², P. Chakraborty⁴⁸, S. Chandra¹⁴¹, B. Chang¹²⁷, W. Chang⁶, S. Chapeland³⁴, M. Chartier¹²⁸, S. Chattopadhyay¹⁴¹, S. Chattopadhyay¹⁰⁸, A. Chauvin²⁴, C. Cheshkov¹³⁵, B. Cheynis¹³⁵, V. Chibante Barroso³⁴, D.D. Chinellato¹²², S. Cho⁶⁰, P. Chochula³⁴, T. Chowdhury¹³⁴, P. Christakoglou⁸⁹, C.H. Christensen⁸⁸, P. Christiansen⁸⁰, T. Chujo¹³³, C. Cicalo⁵⁴, L. Cifarelli^{10,27}, F. Cindolo⁵³, J. Cleymans¹²⁵, F. Colamaria⁵², D. Colella⁵², A. Collu⁷⁹, M. Colocci²⁷, M. Concas^{58,ii}, G. Conesa Balbastre⁷⁸, Z. Conesa del Valle⁶¹, G. Contin¹²⁸, J.G. Contreras³⁷, T.M. Cormier⁹⁴, Y. Corrales Morales^{26,58}, P. Cortese³², M.R. Cosentino¹²³, F. Costa³⁴, S. Costanza¹³⁹, J. Crkovská⁶¹, P. Crochet¹³⁴, E. Cuautle⁷⁰, L. Cunqueiro⁹⁴, D. Dabrowski¹⁴², T. Dahms^{103,117}, A. Dainese⁵⁶, F.P.A. Damas^{137,114}, S. Dani⁶⁶, M.C. Danisch¹⁰², A. Danu⁶⁸, D. Das¹⁰⁸, I. Das¹⁰⁸, S. Das³, A. Dash⁸⁵, S. Dash⁴⁸, A. Dashi¹⁰³, S. De^{85,49}, A. De Caro³⁰, G. de Cataldo⁵², C. de Conti¹²¹, J. de Cuveland³⁹, A. De Falco²⁴, D. De Gruttola¹⁰, N. De Marco⁵⁸, S. De Pasquale³⁰, R.D. De Souza¹²², S. Deb⁴⁹, H.F. Degenhardt¹²¹, A. Deisting^{102,105}, K.R. Deja¹⁴², A. Deloff⁸⁴, S. Delsanto^{131,26}, P. Dhankher⁴⁸, D. Di Bari³³, A. Di Mauro³⁴, R.A. Diaz⁸, T. Dietel¹²⁵, P. Dillenseger⁶⁹, Y. Ding⁶, R. Divià³⁴, Ø. Djuvsland²², U. Dmitrieva⁶², A. Dobrin^{34,68}, D. Domenicis Gimenez¹²¹, B. Dönigus⁶⁹, O. Dordic²¹, A.K. Dubey¹⁴¹, A. Dubla¹⁰⁵, S. Dudi⁹⁸, A.K. Duggal⁹⁸, M. Dukhishyam⁸⁵, P. Dupieux¹³⁴, R.J. Ehlers¹⁴⁶, D. Elia⁵², H. Engel⁷⁴, E. Epple¹⁴⁶, B. Erasmus¹¹⁴, F. Erhardt⁹⁷, A. Erokhin¹¹², M.R. Ersdal²², B. Espagnon⁶¹, G. Eulisse³⁴, J. Eum¹⁸, D. Evans¹⁰⁹, S. Evdokimov⁹⁰, L. Fabbietti^{117,103}, M. Faggin²⁹, J. Faivre⁷⁸, A. Fantoni⁵¹, M. Fasel⁹⁴, P. Fedchio³¹, L. Feldkamp¹⁴⁴, A. Feliciello⁵⁸, G. Feofilov¹¹², A. Fernández Téllez⁴⁴, A. Ferrero¹³⁷, A. Ferretti²⁶, A. Festanti³⁴, V.J.G. Feuillard¹⁰², J. Figiel¹¹⁸, S. Filchagin¹⁰⁷, D. Finogeev⁶², F.M. Fionda²², G. Fiorenza⁵², F. Flor¹²⁶, S. Foertsch⁷³, P. Foka¹⁰⁵, S. Fokin⁸⁷, E. Fragiaco⁵⁹, A. Francisco¹¹⁴, U. Frankfeld¹⁰⁵, G.G. Fronze²⁶, U. Fuchs³⁴, C. Furget⁷⁸, A. Furs⁶², M. Fusco Girard³⁰, J.J. Gaardhøje⁸⁸, M. Gagliardi²⁶, A.M. Gago¹¹⁰, A. Gal¹³⁶, C.D. Galvan¹²⁰, P. Ganoti⁸³, C. Garabatos¹⁰⁵, E. Garcia-Solis¹¹, K. Garg²⁸, C. Gargiulo³⁴, K. Garner¹⁴⁴, P. Gasik^{103,117}, E.F. Gauger¹¹⁹, M.B. Gay Ducati⁷¹, M. Germain¹¹⁴, J. Ghosh¹⁰⁸, P. Ghosh¹⁴¹, S.K. Ghosh³, P. Gianotti⁵¹, P. Giubellino^{105,58}, P. Giubilato²⁹, P. Glässel¹⁰², D.M. Gómez Coral⁷², A. Gomez Ramirez⁷⁴, V. Gonzalez¹⁰⁵, P. González-Zamora⁴⁴, S. Gorbunov³⁹, L. Görlich¹¹⁸, S. Gotovac³⁵, V. Grabski⁷², L.K. Graczykowski¹⁴², K.L. Graham¹⁰⁹, L. Greiner⁷⁹, A. Grelli⁶³, C. Grigoras³⁴, V. Grigoriev⁹¹, A. Grigoryan¹, S. Grigoryan⁷⁵, O.S. Groettvik²², J.M. Gronefeld¹⁰⁵, F. Grosa³¹, J.F. Grosse-Oetringhaus³⁴, R. Grosso¹⁰⁵, R. Guernane⁷⁸, B. Guerzoni²⁷, M. Guittiere¹¹⁴, K. Gulbrandsen⁸⁸, T. Gunji¹³², A. Gupta⁹⁹, R. Gupta⁹⁹, I.B. Guzman⁴⁴, R. Haake^{146,34}, M.K. Habib¹⁰⁵, C. Hadjidakis⁶¹, H. Hamagaki⁸¹, G. Hamar¹⁴⁵, M. Hamid⁶, J.C. Hamon¹³⁶, R. Hannigan¹¹⁹, M.R. Haque⁶³, A. Harlanderova¹⁰⁵, J.W. Harris¹⁴⁶, A. Harton¹¹, H. Hassan⁷⁸, D. Hatzifotiadou^{10,53}, P. Hauer⁴², S. Hayashi¹³², S.T. Heckel⁶⁹, E. Hellbär⁶⁹, H. Helstrup³⁶, A. Hergheliegiu⁴⁷, E.G. Hernandez⁴⁴, G. Herrera Corral⁹, F. Herrmann¹⁴⁴, K.F. Hetland³⁶, T.E. Hilden⁴³, H. Hillemanns³⁴, C. Hills¹²⁸, B. Hippolyte¹³⁶, B. Hohlweger¹⁰³, D. Horak³⁷, S. Hornung¹⁰⁵, R. Hosokawa¹³³,

P. Hristov³⁴, C. Huang⁶¹, C. Hughes¹³⁰, P. Huhn⁶⁹, T.J. Humanic⁹⁵, H. Hushnud¹⁰⁸, L.A. Husova¹⁴⁴, N. Hussain⁴¹, S.A. Hussain¹⁵, T. Hussain¹⁷, D. Hutter³⁹, D.S. Hwang¹⁹, J.P. Iddon¹²⁸, R. Ilkaev¹⁰⁷, M. Inaba¹³³, M. Ippolitov⁸⁷, M.S. Islam¹⁰⁸, M. Ivanov¹⁰⁵, V. Ivanov⁹⁶, V. Izucheev⁹⁰, B. Jacak⁷⁹, N. Jacazio²⁷, P.M. Jacobs⁷⁹, M.B. Jadhav⁴⁸, S. Jadlovská¹¹⁶, J. Jadlovsky¹¹⁶, S. Jaelani⁶³, C. Jahnke¹²¹, M.J. Jakubowska¹⁴², M.A. Janik¹⁴², M. Jercic⁹⁷, O. Jevons¹⁰⁹, R.T. Jimenez Bustamante¹⁰⁵, M. Jin¹²⁶, F. Jonas^{144,94}, P.G. Jones¹⁰⁹, A. Jusko¹⁰⁹, P. Kalinak⁶⁵, A. Kalweit³⁴, J.H. Kang¹⁴⁷, V. Kaplin⁹¹, S. Kar⁶, A. Karasu Uysal⁷⁷, O. Karavichev⁶², T. Karavicheva⁶², P. Karczmarczyk³⁴, E. Karpechev⁶², U. Kebschull⁷⁴, R. Keidel⁴⁶, M. Keil³⁴, B. Ketzer⁴², Z. Khabanova⁸⁹, A.M. Khan⁶, S. Khan¹⁷, S.A. Khan¹⁴¹, A. Khanzadeev⁹⁶, Y. Kharlov⁹⁰, A. Khatun¹⁷, A. Khuntia^{118,49}, B. Kileng³⁶, B. Kim⁶⁰, B. Kim¹³³, D. Kim¹⁴⁷, D.J. Kim¹²⁷, E.J. Kim¹³, H. Kim¹⁴⁷, J.S. Kim⁴⁰, J. Kim¹⁰², J. Kim¹⁴⁷, J. Kim¹³, M. Kim^{60,102}, S. Kim¹⁹, T. Kim¹⁴⁷, T. Kim¹⁴⁷, K. Kindra⁹⁸, S. Kirsch³⁹, I. Kisel³⁹, S. Kiselev⁶⁴, A. Kisiel¹⁴², J.L. Klay⁵, C. Klein⁶⁹, J. Klein⁵⁸, S. Klein⁷⁹, C. Klein-Bösing¹⁴⁴, S. Klewin¹⁰², A. Kluge³⁴, M.L. Knichel³⁴, A.G. Knospe¹²⁶, C. Kobdaj¹¹⁵, M.K. Köhler¹⁰², T. Kollegger¹⁰⁵, A. Kondratyev⁷⁵, N. Kondratyeva⁹¹, E. Kondratyuk⁹⁰, P.J. Konopka³⁴, M. Konyushikhin¹⁴³, L. Koska¹¹⁶, O. Kovalenko⁸⁴, V. Kovalenko¹¹², M. Kowalski¹¹⁸, I. Králik⁶⁵, A. Kravčáková³⁸, L. Kreis¹⁰⁵, M. Krivda^{65,109}, F. Krizek⁹³, K. Krizkova Gajdosova³⁷, M. Krüger⁶⁹, E. Kryshen⁹⁶, M. Krzewicki³⁹, A.M. Kubera⁹⁵, V. Kučera⁶⁰, C. Kuhn¹³⁶, P.G. Kuijjer⁸⁹, L. Kumar⁹⁸, S. Kumar⁴⁸, S. Kundu⁸⁵, P. Kurashvili⁸⁴, A. Kurepin⁶², A.B. Kurepin⁶², S. Kushpil⁹³, J. Kvapil¹⁰⁹, M.J. Kweon⁶⁰, Y. Kwon¹⁴⁷, S.L. La Pointe³⁹, P. La Rocca²⁸, Y.S. Lai⁷⁹, R. Langoy¹²⁴, K. Lapidus^{34,146}, A. Lardeux²¹, P. Larionov⁵¹, E. Laudi³⁴, R. Lavicka³⁷, T. Lazareva¹¹², R. Lea²⁵, L. Leardini¹⁰², S. Lee¹⁴⁷, F. Lehas⁸⁹, S. Lehner¹¹³, J. Lehrbach³⁹, R.C. Lemmon⁹², I. León Monzón¹²⁰, E.D. Lesser²⁰, M. Lettrich³⁴, P. Lévai¹⁴⁵, X. Li¹², X.L. Li⁶, J. Lien¹²⁴, R. Lietava¹⁰⁹, B. Lim¹⁸, S. Lindal²¹, V. Lindenstruth³⁹, S.W. Lindsay¹²⁸, C. Lippmann¹⁰⁵, M.A. Lisa⁹⁵, V. Litychovskiy⁴³, A. Liu⁷⁹, S. Liu⁹⁵, H.M. Ljunggren⁸⁰, W.J. Llope¹⁴³, I.M. Lofnes²², V. Loginov⁹¹, C. Loizides⁹⁴, P. Loncar³⁵, X. Lopez¹³⁴, E. López Torres⁸, P. Luettig⁶⁹, J.R. Luhder¹⁴⁴, M. Lunardon²⁹, G. Luparello⁵⁹, M. Lupi³⁴, A. Maevskaya⁶², M. Mager³⁴, S.M. Mahmood²¹, T. Mahmoud⁴², A. Maire¹³⁶, R.D. Majka¹⁴⁶, M. Malaev⁹⁶, Q.W. Malik²¹, L. Malinina^{75,iii}, D. Mal'Kevich⁶⁴, P. Malzacher¹⁰⁵, A. Mamonov¹⁰⁷, V. Manko⁸⁷, F. Manso¹³⁴, V. Manzarí⁵², Y. Mao⁶, M. Marchisone¹³⁵, J. Mareš⁶⁷, G.V. Margagliotti²⁵, A. Margotti⁵³, J. Margutti⁶³, A. Marín¹⁰⁵, C. Markert¹¹⁹, M. Marquard⁶⁹, N.A. Martin¹⁰², P. Martinengo³⁴, J.L. Martinez¹²⁶, M.I. Martínez⁴⁴, G. Martínez García¹¹⁴, M. Martínez Pedreira³⁴, S. Masciocchi¹⁰⁵, M. Masera²⁶, A. Masoni⁵⁴, L. Massacrier⁶¹, E. Masson¹¹⁴, A. Mastroserio^{52,138}, A.M. Mathis^{103,117}, P.F.T. Matuoka¹²¹, A. Matyja¹¹⁸, C. Mayer¹¹⁸, M. Mazzilli³³, M.A. Mazzoni⁵⁷, A.F. Mechler⁶⁹, F. Meddi²³, Y. Melikyan⁹¹, A. Menchaca-Rocha⁷², E. Meninno³⁰, M. Meres¹⁴, S. Mhlanga¹²⁵, Y. Miake¹³³, L. Micheletti²⁶, M.M. Mieskolainen⁴³, D.L. Mihaylov¹⁰³, K. Mikhaylov^{64,75}, A. Mischke^{63,i}, A.N. Mishra⁷⁰, D. Miśkowiec¹⁰⁵, C.M. Mitu⁶⁸, N. Mohammadi³⁴, A.P. Mohanty⁶³, B. Mohanty⁸⁵, M. Mohisin Khan^{17,iv}, M. Mondal¹⁴¹, M.M. Mondal⁶⁶, C. Mordasini¹⁰³, D.A. Moreira De Godoy¹⁴⁴, L.A.P. Moreno⁴⁴, S. Moretto²⁹, A. Morreale¹¹⁴, A. Morsch³⁴, T. Mrnjavac³⁴, V. Muccifora⁵¹, E. Mudnic³⁵, D. Mühlheim¹⁴⁴, S. Muhuri¹⁴¹, J.D. Mulligan^{79,146}, M.G. Munhoz¹²¹, K. Munning⁴², R.H. Munzer⁶⁹, H. Murakami¹³², S. Murray⁷³, L. Musa³⁴, J. Musinsky⁶⁵, C.J. Myers¹²⁶, J.W. Myrcha¹⁴², B. Naik⁴⁸, R. Nair⁸⁴, B.K. Nandi⁴⁸, R. Nania^{10,53}, E. Nappi⁵², M.U. Naru¹⁵, A.F. Nassirpour⁸⁰, H. Natal da Luz¹²¹, C. Nattrass¹³⁰, R. Nayak⁴⁸, T.K. Nayak^{141,85}, S. Nazarenko¹⁰⁷, R.A. Negrao De Oliveira⁶⁹, L. Nellen⁷⁰, S.V. Nesbo³⁶, G. Neskovic³⁹, J. Niedziela^{142,34}, B.S. Nielsen⁸⁸, S. Nikolaev⁸⁷, S. Nikulin⁸⁷, V. Nikulin⁹⁶, F. Noferini^{10,53}, P. Nomokonov⁷⁵, G. Nooren⁶³, J. Norman⁷⁸, P. Nowakowski¹⁴², A. Nyanin⁸⁷, J. Nystrand²², M. Ogino⁸¹, A. Ohlson¹⁰², J. Oleniacz¹⁴², A.C. Oliveira Da Silva¹²¹, M.H. Oliver¹⁴⁶, J. Onderwaater¹⁰⁵, C. Oppedisano⁵⁸, R. Orava⁴³, A. Ortiz Velasquez⁷⁰, A. Oskarsson⁸⁰, J. Otwinowski¹¹⁸, K. Oyama⁸¹, Y. Pachmayer¹⁰², V. Pacik⁸⁸, D. Pagano¹⁴⁰, G. Paic⁷⁰, P. Palni⁶, J. Pan¹⁴³, A.K. Pandey⁴⁸, S. Panebianco¹³⁷, V. Papikyan¹, P. Pareek⁴⁹, J. Park⁶⁰, J.E. Parkkila¹²⁷, S. Parmar⁹⁸, A. Passfeld¹⁴⁴, S.P. Pathak¹²⁶, R.N. Patra¹⁴¹, B. Paul⁵⁸, H. Pei⁶, T. Peitzmann⁶³, X. Peng⁶, L.G. Pereira⁷¹, H. Pereira Da Costa¹³⁷, D. Peresunko⁸⁷, G.M. Perez⁸, E. Perez Lezama⁶⁹, V. Peskov⁶⁹, Y. Pestov⁴, V. Petráček³⁷, M. Petrovici⁴⁷, R.P. Pezzi⁷¹, S. Piano⁵⁹, M. Pikna¹⁴, P. Pillot¹¹⁴, L.O.D.L. Pimentel⁸⁸, O. Pinazza^{53,34}, L. Pinsky¹²⁶, S. Pisano⁵¹, D.B. Piyarathna¹²⁶, M. Płoskoń⁷⁹, M. Planinic⁹⁷, F. Pliquett⁶⁹, J. Pluta¹⁴², S. Pochybova¹⁴⁵, M.G. Poghosyan⁹⁴, B. Polichtchouk⁹⁰, N. Poljak⁹⁷, W. Poonsawat¹¹⁵, A. Pop⁴⁷, H. Poppenborg¹⁴⁴, S. Porteboeuf-Houssais¹³⁴, V. Pozdniakov⁷⁵, S.K. Prasad³, R. Preghenella⁵³, F. Prino⁵⁸, C.A. Pruneau¹⁴³, I. Pshenichnov⁶², M. Puccio^{26,34}, V. Punin¹⁰⁷, K. Puranapanda¹⁴¹, J. Putschke¹⁴³, R.E. Quishpe¹²⁶, S. Ragoni¹⁰⁹, S. Raha³, S. Rajput⁹⁹, J. Rak¹²⁷, A. Rakotozafindrabe¹³⁷, L. Ramello³², F. Rami¹³⁶, R. Raniwala¹⁰⁰, S. Raniwala¹⁰⁰, S.S. Räsänen⁴³, B.T. Rascanu⁶⁹, R. Rath⁴⁹, V. Ratza⁴², I. Ravasenga³¹, K.F. Read^{94,130}, K. Redlich^{84,v}, A. Rehman²², P. Reichelt⁶⁹, F. Reidt³⁴, X. Ren⁶, R. Renfordt⁶⁹, A. Reshetin⁶², J.-P. Revol¹⁰, K. Reygers¹⁰²,

V. Riabov⁹⁶, T. Richert^{80,88}, M. Richter²¹, P. Riedler³⁴, W. Riegler³⁴, F. Riggi²⁸, C. Ristea⁶⁸, S.P. Rode⁴⁹, M. Rodríguez Cahuantzi⁴⁴, K. Røed²¹, R. Rogalev⁹⁰, E. Rogochaya⁷⁵, D. Rohr³⁴, D. Röhrich²², P.S. Rokita¹⁴², F. Ronchetti⁵¹, E.D. Rosas⁷⁰, K. Roslon¹⁴², P. Rosnet¹³⁴, A. Rossi^{56,29}, A. Rotondi¹³⁹, F. Roukoutakis⁸³, A. Roy⁴⁹, P. Roy¹⁰⁸, O.V. Rueda⁸⁰, R. Rui²⁵, B. Rumyantsev⁷⁵, A. Rustamov⁸⁶, E. Ryabinkin⁸⁷, Y. Ryabov⁹⁶, A. Rybicki¹¹⁸, H. Rytkonen¹²⁷, S. Saarinen⁴³, S. Sadhu¹⁴¹, S. Sadovsky⁹⁰, K. Šafařík^{34,37}, S.K. Saha¹⁴¹, B. Sahoo⁴⁸, P. Sahoo⁴⁹, R. Sahoo⁴⁹, S. Sahoo⁶⁶, P.K. Sahu⁶⁶, J. Saini¹⁴¹, S. Sakai¹³³, S. Sambyal⁹⁹, V. Samsonov^{96,91}, A. Sandoval⁷², A. Sarkar⁷³, D. Sarkar^{143,141}, N. Sarkar¹⁴¹, P. Sarma⁴¹, V.M. Sarti¹⁰³, M.H.P. Sas⁶³, E. Scapparone⁵³, B. Schaefer⁹⁴, J. Schambach¹¹⁹, H.S. Scheid⁶⁹, C. Schiaua⁴⁷, R. Schicker¹⁰², A. Schmah¹⁰², C. Schmidt¹⁰⁵, H.R. Schmidt¹⁰¹, M.O. Schmidt¹⁰², M. Schmidt¹⁰¹, N.V. Schmidt^{94,69}, A.R. Schmier¹³⁰, J. Schukraft^{88,34}, Y. Schutz^{34,136}, K. Schwarz¹⁰⁵, K. Schweda¹⁰⁵, G. Scioli²⁷, E. Scomparin⁵⁸, M. Šefčík³⁸, J.E. Seger¹⁶, Y. Sekiguchi¹³², D. Sekihata⁴⁵, I. Selyuzhenkov^{91,105}, S. Senyukov¹³⁶, E. Serradilla⁷², P. Sett⁴⁸, A. Sevcenco⁶⁸, A. Shabanov⁶², A. Shabetai¹¹⁴, R. Shahoyan³⁴, W. Shaikh¹⁰⁸, A. Shangaraev⁹⁰, A. Sharma⁹⁸, A. Sharma⁹⁹, M. Sharma⁹⁹, N. Sharma⁹⁸, A.I. Sheikh¹⁴¹, K. Shigaki⁴⁵, M. Shimomura⁸², S. Shirinkin⁶⁴, Q. Shou¹¹¹, Y. Sibiriyak⁸⁷, S. Siddhanta⁵⁴, T. Siemiarczuk⁸⁴, D. Silvermyr⁸⁰, G. Simatovic⁸⁹, G. Simonetti^{34,103}, R. Singh⁸⁵, R. Singh⁹⁹, V.K. Singh¹⁴¹, V. Singhal¹⁴¹, T. Sinha¹⁰⁸, B. Sitar¹⁴, M. Sitta³², T.B. Skaali²¹, M. Slupecki¹²⁷, N. Smirnov¹⁴⁶, R.J.M. Snellings⁶³, T.W. Snellman¹²⁷, J. Sochan¹¹⁶, C. Soncco¹¹⁰, A. Songmoolnak¹¹⁵, F. Soramel²⁹, S. Sorensen¹³⁰, I. Sputowska¹¹⁸, J. Stachel¹⁰², I. Stan⁶⁸, P. Stankus⁹⁴, P.J. Steffanic¹³⁰, E. Stenlund⁸⁰, D. Stocco¹¹⁴, M.M. Storetvedt³⁶, P. Strmen¹⁴, A.A.P. Suaide¹²¹, T. Sugitate⁴⁵, C. Suire⁶¹, M. Suleymanov¹⁵, M. Suljic³⁴, R. Sultanov⁶⁴, M. Šumbera⁹³, S. Sumowidagdo⁵⁰, K. Suzuki¹¹³, S. Swain⁶⁶, A. Szabo¹⁴, I. Szarka¹⁴, U. Tabassam¹⁵, G. Taillepied¹³⁴, J. Takahashi¹²², G.J. Tambave²², S. Tang⁶, M. Tarhini¹¹⁴, M.G. Tarzila⁴⁷, A. Tauro³⁴, G. Tejada Muñoz⁴⁴, A. Telesca³⁴, C. Terrevoli^{126,29}, D. Thakur⁴⁹, S. Thakur¹⁴¹, D. Thomas¹¹⁹, F. Thoresen⁸⁸, R. Tieulent¹³⁵, A. Tikhonov⁶², A.R. Timmins¹²⁶, A. Toia⁶⁹, N. Topilskaya⁶², M. Toppi⁵¹, F. Torres-Acosta²⁰, S.R. Torres¹²⁰, S. Tripathy⁴⁹, T. Tripathy⁴⁸, S. Trogolo^{26,29}, G. Trombetta³³, L. Tropp³⁸, V. Trubnikov², W.H. Trzaska¹²⁷, T.P. Trzcinski¹⁴², B.A. Trzeciak⁶³, T. Tsuji¹³², A. Tumkin¹⁰⁷, R. Turrisi⁵⁶, T.S. Tveter²¹, K. Ullaland²², E.N. Umaka¹²⁶, A. Uras¹³⁵, G.L. Usai²⁴, A. Utrobicic⁹⁷, M. Vala^{116,38}, N. Valle¹³⁹, S. Vallero⁵⁸, N. van der Kolk⁶³, L.V.R. van Doremalen⁶³, M. van Leeuwen⁶³, P. Vande Vyvre³⁴, D. Varga¹⁴⁵, M. Varga-Kofarago¹⁴⁵, A. Vargas⁴⁴, M. Vargyas¹²⁷, R. Varma⁴⁸, M. Vasileiou⁸³, A. Vasiliev⁸⁷, O. Vázquez Doce^{117,103}, V. Vechernin¹¹², A.M. Veen⁶³, E. Vercellin²⁶, S. Vergara Limón⁴⁴, L. Vermunt⁶³, R. Vernet⁷, R. Vértesi¹⁴⁵, L. Vickovic³⁵, J. Viinikainen¹²⁷, Z. Vilakazi¹³¹, O. Villalobos Baillie¹⁰⁹, A. Villatoro Tello⁴⁴, G. Vino⁵², A. Vinogradov⁸⁷, T. Virgili³⁰, V. Vislavicius⁸⁸, A. Vodopyanov⁷⁵, B. Volkel³⁴, M.A. Völkl¹⁰¹, K. Voloshin⁶⁴, S.A. Voloshin¹⁴³, G. Volpe³³, B. von Haller³⁴, I. Vorobyev^{103,117}, D. Voscek¹¹⁶, J. Vrláková³⁸, B. Wagner²², Y. Watanabe¹³³, M. Weber¹¹³, S.G. Weber¹⁰⁵, A. Wegrzynek³⁴, D.F. Weiser¹⁰², S.C. Wenzel³⁴, J.P. Wessels¹⁴⁴, U. Westerhoff¹⁴⁴, A.M. Whitehead¹²⁵, E. Widmann¹¹³, J. Wiechula⁶⁹, J. Wikne²¹, G. Wilk⁸⁴, J. Wilkinson⁵³, G.A. Willems³⁴, E. Willsher¹⁰⁹, B. Windelband¹⁰², W.E. Witt¹³⁰, Y. Wu¹²⁹, R. Xu⁶, S. Yalcin⁷⁷, K. Yamakawa⁴⁵, S. Yang²², S. Yano¹³⁷, Z. Yin⁶, H. Yokoyama⁶³, I.-K. Yoo¹⁸, J.H. Yoon⁶⁰, S. Yuan²², A. Yuncu¹⁰², V. Yurchenko², V. Zaccolo^{58,25}, A. Zaman¹⁵, C. Zampolli³⁴, H.J.C. Zanolli¹²¹, N. Zardoshti^{34,109}, A. Zarochentsev¹¹², P. Závada⁶⁷, N. Zaviyalov¹⁰⁷, H. Zbroszczyk¹⁴², M. Zhalov⁹⁶, X. Zhang⁶, Z. Zhang^{6,134}, C. Zhao²¹, V. Zherebchevskii¹¹², N. Zhigareva⁶⁴, D. Zhou⁶, Y. Zhou⁸⁸, Z. Zhou²², J. Zhu⁶, Y. Zhu⁶, A. Zichichi^{27,10}, M.B. Zimmermann³⁴, G. Zinovjev², N. Zurlo¹⁴⁰,

Affiliation notes

ⁱ Deceased

ⁱⁱ Dipartimento DET del Politecnico di Torino, Turin, Italy

ⁱⁱⁱ M.V. Lomonosov Moscow State University, D.V. Skobeltsyn Institute of Nuclear, Physics, Moscow, Russia

^{iv} Department of Applied Physics, Aligarh Muslim University, Aligarh, India

^v Institute of Theoretical Physics, University of Wrocław, Poland

Collaboration Institutes

¹ A.I. Alikhanyan National Science Laboratory (Yerevan Physics Institute) Foundation, Yerevan, Armenia

² Bogolyubov Institute for Theoretical Physics, National Academy of Sciences of Ukraine, Kiev, Ukraine

³ Bose Institute, Department of Physics and Centre for Astroparticle Physics and Space Science (CAPSS), Kolkata, India

⁴ Budker Institute for Nuclear Physics, Novosibirsk, Russia

- ⁵ California Polytechnic State University, San Luis Obispo, California, United States
- ⁶ Central China Normal University, Wuhan, China
- ⁷ Centre de Calcul de l'IN2P3, Villeurbanne, Lyon, France
- ⁸ Centro de Aplicaciones Tecnológicas y Desarrollo Nuclear (CEADEN), Havana, Cuba
- ⁹ Centro de Investigación y de Estudios Avanzados (CINVESTAV), Mexico City and Mérida, Mexico
- ¹⁰ Centro Fermi - Museo Storico della Fisica e Centro Studi e Ricerche "Enrico Fermi", Rome, Italy
- ¹¹ Chicago State University, Chicago, Illinois, United States
- ¹² China Institute of Atomic Energy, Beijing, China
- ¹³ Chonbuk National University, Jeonju, Republic of Korea
- ¹⁴ Comenius University Bratislava, Faculty of Mathematics, Physics and Informatics, Bratislava, Slovakia
- ¹⁵ COMSATS University Islamabad, Islamabad, Pakistan
- ¹⁶ Creighton University, Omaha, Nebraska, United States
- ¹⁷ Department of Physics, Aligarh Muslim University, Aligarh, India
- ¹⁸ Department of Physics, Pusan National University, Pusan, Republic of Korea
- ¹⁹ Department of Physics, Sejong University, Seoul, Republic of Korea
- ²⁰ Department of Physics, University of California, Berkeley, California, United States
- ²¹ Department of Physics, University of Oslo, Oslo, Norway
- ²² Department of Physics and Technology, University of Bergen, Bergen, Norway
- ²³ Dipartimento di Fisica dell'Università 'La Sapienza' and Sezione INFN, Rome, Italy
- ²⁴ Dipartimento di Fisica dell'Università and Sezione INFN, Cagliari, Italy
- ²⁵ Dipartimento di Fisica dell'Università and Sezione INFN, Trieste, Italy
- ²⁶ Dipartimento di Fisica dell'Università and Sezione INFN, Turin, Italy
- ²⁷ Dipartimento di Fisica e Astronomia dell'Università and Sezione INFN, Bologna, Italy
- ²⁸ Dipartimento di Fisica e Astronomia dell'Università and Sezione INFN, Catania, Italy
- ²⁹ Dipartimento di Fisica e Astronomia dell'Università and Sezione INFN, Padova, Italy
- ³⁰ Dipartimento di Fisica 'E.R. Caianiello' dell'Università and Gruppo Collegato INFN, Salerno, Italy
- ³¹ Dipartimento DISAT del Politecnico and Sezione INFN, Turin, Italy
- ³² Dipartimento di Scienze e Innovazione Tecnologica dell'Università del Piemonte Orientale and INFN Sezione di Torino, Alessandria, Italy
- ³³ Dipartimento Interateneo di Fisica 'M. Merlin' and Sezione INFN, Bari, Italy
- ³⁴ European Organization for Nuclear Research (CERN), Geneva, Switzerland
- ³⁵ Faculty of Electrical Engineering, Mechanical Engineering and Naval Architecture, University of Split, Split, Croatia
- ³⁶ Faculty of Engineering and Science, Western Norway University of Applied Sciences, Bergen, Norway
- ³⁷ Faculty of Nuclear Sciences and Physical Engineering, Czech Technical University in Prague, Prague, Czech Republic
- ³⁸ Faculty of Science, P.J. Šafárik University, Košice, Slovakia
- ³⁹ Frankfurt Institute for Advanced Studies, Johann Wolfgang Goethe-Universität Frankfurt, Frankfurt, Germany
- ⁴⁰ Gangneung-Wonju National University, Gangneung, Republic of Korea
- ⁴¹ Gauhati University, Department of Physics, Guwahati, India
- ⁴² Helmholtz-Institut für Strahlen- und Kernphysik, Rheinische Friedrich-Wilhelms-Universität Bonn, Bonn, Germany
- ⁴³ Helsinki Institute of Physics (HIP), Helsinki, Finland
- ⁴⁴ High Energy Physics Group, Universidad Autónoma de Puebla, Puebla, Mexico
- ⁴⁵ Hiroshima University, Hiroshima, Japan
- ⁴⁶ Hochschule Worms, Zentrum für Technologietransfer und Telekommunikation (ZTT), Worms, Germany
- ⁴⁷ Horia Hulubei National Institute of Physics and Nuclear Engineering, Bucharest, Romania
- ⁴⁸ Indian Institute of Technology Bombay (IIT), Mumbai, India
- ⁴⁹ Indian Institute of Technology Indore, Indore, India
- ⁵⁰ Indonesian Institute of Sciences, Jakarta, Indonesia
- ⁵¹ INFN, Laboratori Nazionali di Frascati, Frascati, Italy
- ⁵² INFN, Sezione di Bari, Bari, Italy
- ⁵³ INFN, Sezione di Bologna, Bologna, Italy
- ⁵⁴ INFN, Sezione di Cagliari, Cagliari, Italy
- ⁵⁵ INFN, Sezione di Catania, Catania, Italy

- 56 INFN, Sezione di Padova, Padova, Italy
- 57 INFN, Sezione di Roma, Rome, Italy
- 58 INFN, Sezione di Torino, Turin, Italy
- 59 INFN, Sezione di Trieste, Trieste, Italy
- 60 Inha University, Incheon, Republic of Korea
- 61 Institut de Physique Nucléaire d'Orsay (IPNO), Institut National de Physique Nucléaire et de Physique des Particules (IN2P3/CNRS), Université de Paris-Sud, Université Paris-Saclay, Orsay, France
- 62 Institute for Nuclear Research, Academy of Sciences, Moscow, Russia
- 63 Institute for Subatomic Physics, Utrecht University/Nikhef, Utrecht, Netherlands
- 64 Institute for Theoretical and Experimental Physics, Moscow, Russia
- 65 Institute of Experimental Physics, Slovak Academy of Sciences, Košice, Slovakia
- 66 Institute of Physics, Homi Bhabha National Institute, Bhubaneswar, India
- 67 Institute of Physics of the Czech Academy of Sciences, Prague, Czech Republic
- 68 Institute of Space Science (ISS), Bucharest, Romania
- 69 Institut für Kernphysik, Johann Wolfgang Goethe-Universität Frankfurt, Frankfurt, Germany
- 70 Instituto de Ciencias Nucleares, Universidad Nacional Autónoma de México, Mexico City, Mexico
- 71 Instituto de Física, Universidade Federal do Rio Grande do Sul (UFRGS), Porto Alegre, Brazil
- 72 Instituto de Física, Universidad Nacional Autónoma de México, Mexico City, Mexico
- 73 iThemba LABS, National Research Foundation, Somerset West, South Africa
- 74 Johann-Wolfgang-Goethe Universität Frankfurt Institut für Informatik, Fachbereich Informatik und Mathematik, Frankfurt, Germany
- 75 Joint Institute for Nuclear Research (JINR), Dubna, Russia
- 76 Korea Institute of Science and Technology Information, Daejeon, Republic of Korea
- 77 KTO Karatay University, Konya, Turkey
- 78 Laboratoire de Physique Subatomique et de Cosmologie, Université Grenoble-Alpes, CNRS-IN2P3, Grenoble, France
- 79 Lawrence Berkeley National Laboratory, Berkeley, California, United States
- 80 Lund University Department of Physics, Division of Particle Physics, Lund, Sweden
- 81 Nagasaki Institute of Applied Science, Nagasaki, Japan
- 82 Nara Women's University (NWU), Nara, Japan
- 83 National and Kapodistrian University of Athens, School of Science, Department of Physics, Athens, Greece
- 84 National Centre for Nuclear Research, Warsaw, Poland
- 85 National Institute of Science Education and Research, Homi Bhabha National Institute, Jatni, India
- 86 National Nuclear Research Center, Baku, Azerbaijan
- 87 National Research Centre Kurchatov Institute, Moscow, Russia
- 88 Niels Bohr Institute, University of Copenhagen, Copenhagen, Denmark
- 89 Nikhef, National institute for subatomic physics, Amsterdam, Netherlands
- 90 NRC Kurchatov Institute IHEP, Protvino, Russia
- 91 NRNU Moscow Engineering Physics Institute, Moscow, Russia
- 92 Nuclear Physics Group, STFC Daresbury Laboratory, Daresbury, United Kingdom
- 93 Nuclear Physics Institute of the Czech Academy of Sciences, Řež u Prahy, Czech Republic
- 94 Oak Ridge National Laboratory, Oak Ridge, Tennessee, United States
- 95 Ohio State University, Columbus, Ohio, United States
- 96 Petersburg Nuclear Physics Institute, Gatchina, Russia
- 97 Physics department, Faculty of science, University of Zagreb, Zagreb, Croatia
- 98 Physics Department, Panjab University, Chandigarh, India
- 99 Physics Department, University of Jammu, Jammu, India
- 100 Physics Department, University of Rajasthan, Jaipur, India
- 101 Physikalisches Institut, Eberhard-Karls-Universität Tübingen, Tübingen, Germany
- 102 Physikalisches Institut, Ruprecht-Karls-Universität Heidelberg, Heidelberg, Germany
- 103 Physik Department, Technische Universität München, Munich, Germany
- 104 Politecnico di Bari, Bari, Italy
- 105 Research Division and ExtreMe Matter Institute EMMI, GSI Helmholtzzentrum für Schwerionenforschung GmbH, Darmstadt, Germany
- 106 Rudjer Bošković Institute, Zagreb, Croatia

- 107 Russian Federal Nuclear Center (VNIIEF), Sarov, Russia
- 108 Saha Institute of Nuclear Physics, Homi Bhabha National Institute, Kolkata, India
- 109 School of Physics and Astronomy, University of Birmingham, Birmingham, United Kingdom
- 110 Sección Física, Departamento de Ciencias, Pontificia Universidad Católica del Perú, Lima, Peru
- 111 Shanghai Institute of Applied Physics, Shanghai, China
- 112 St. Petersburg State University, St. Petersburg, Russia
- 113 Stefan Meyer Institut für Subatomare Physik (SMI), Vienna, Austria
- 114 SUBATECH, IMT Atlantique, Université de Nantes, CNRS-IN2P3, Nantes, France
- 115 Suranaree University of Technology, Nakhon Ratchasima, Thailand
- 116 Technical University of Košice, Košice, Slovakia
- 117 Technische Universität München, Excellence Cluster 'Universe', Munich, Germany
- 118 The Henryk Niewodniczanski Institute of Nuclear Physics, Polish Academy of Sciences, Cracow, Poland
- 119 The University of Texas at Austin, Austin, Texas, United States
- 120 Universidad Autónoma de Sinaloa, Culiacán, Mexico
- 121 Universidade de São Paulo (USP), São Paulo, Brazil
- 122 Universidade Estadual de Campinas (UNICAMP), Campinas, Brazil
- 123 Universidade Federal do ABC, Santo Andre, Brazil
- 124 University College of Southeast Norway, Tonsberg, Norway
- 125 University of Cape Town, Cape Town, South Africa
- 126 University of Houston, Houston, Texas, United States
- 127 University of Jyväskylä, Jyväskylä, Finland
- 128 University of Liverpool, Liverpool, United Kingdom
- 129 University of Science and Technology of China, Hefei, China
- 130 University of Tennessee, Knoxville, Tennessee, United States
- 131 University of the Witwatersrand, Johannesburg, South Africa
- 132 University of Tokyo, Tokyo, Japan
- 133 University of Tsukuba, Tsukuba, Japan
- 134 Université Clermont Auvergne, CNRS/IN2P3, LPC, Clermont-Ferrand, France
- 135 Université de Lyon, Université Lyon 1, CNRS/IN2P3, IPN-Lyon, Villeurbanne, Lyon, France
- 136 Université de Strasbourg, CNRS, IPHC UMR 7178, F-67000 Strasbourg, France, Strasbourg, France
- 137 Université Paris-Saclay Centre d'Etudes de Saclay (CEA), IRFU, Département de Physique Nucléaire (DPhN), Saclay, France
- 138 Università degli Studi di Foggia, Foggia, Italy
- 139 Università degli Studi di Pavia, Pavia, Italy
- 140 Università di Brescia, Brescia, Italy
- 141 Variable Energy Cyclotron Centre, Homi Bhabha National Institute, Kolkata, India
- 142 Warsaw University of Technology, Warsaw, Poland
- 143 Wayne State University, Detroit, Michigan, United States
- 144 Westfälische Wilhelms-Universität Münster, Institut für Kernphysik, Münster, Germany
- 145 Wigner Research Centre for Physics, Hungarian Academy of Sciences, Budapest, Hungary
- 146 Yale University, New Haven, Connecticut, United States
- 147 Yonsei University, Seoul, Republic of Korea